

Exact 3D solutions and finite element 2D models for free vibration analysis of plates and cylinders

Original

Exact 3D solutions and finite element 2D models for free vibration analysis of plates and cylinders / Brischetto, Salvatore; Torre, Roberto. - In: CURVED AND LAYERED STRUCTURES. - ISSN 2353-7396. - 1:1(2014), pp. 59-92. [10.2478/cls-2014-0004]

Availability:

This version is available at: 11583/2982745 since: 2023-10-04T08:53:18Z

Publisher:

DE GRUYTER

Published

DOI:10.2478/cls-2014-0004

Terms of use:

This article is made available under terms and conditions as specified in the corresponding bibliographic description in the repository

Publisher copyright

(Article begins on next page)

Salvatore Brischetto* and Roberto Torre

Exact 3D solutions and finite element 2D models for free vibration analysis of plates and cylinders

Abstract: The paper proposes a comparison between classical two-dimensional (2D) finite elements (FEs) and an exact three-dimensional (3D) solution for the free vibration analysis of one-layered and multilayered isotropic, composite and sandwich plates and cylinders. Low and high order frequencies are analyzed for thick and thin simply supported structures. Vibration modes are investigated to make a comparison between results obtained via the finite element method and those obtained by means of the exact three-dimensional solution. The 3D exact solution is based on the differential equations of equilibrium written in general orthogonal curvilinear coordinates. This exact method is based on a layer-wise approach, the continuity of displacements and transverse shear/normal stresses is imposed at the interfaces between the layers of the structure. The geometry for shells is considered without any simplifications. The 2D finite element results are obtained by means of a well-known commercial FE code. The differences between 2D FE solutions and 3D exact solutions depend on the considered mode, the order of frequency, the thickness ratio of the structure, the geometry, the embedded material and the lamination sequence.

Keywords: plates, shells, finite element method, exact three-dimensional solution, free vibrations, vibration modes

DOI 10.2478/cls-2014-0004

Received September 23, 2014 ; accepted October 20, 2014

1 Introduction


The present paper investigates low and high frequencies in the case of free vibration response of simply-supported

one-layered and multilayered isotropic, composite and sandwich plates and cylinders. The behavior and design of vibrating shells and plates have been extensively discussed in the reports by Leissa [1, 2] and more recently in the book by Werner [3] and in the work by Brischetto and Carrera [4], among others.

The main aim of this work is the comparison between results obtained by means of an exact three-dimensional (3D) solution and those obtained by means of the classical two-dimensional (2D) finite element method (FEM). The proposed exact 3D solution has been developed by Brischetto in [5]-[7] where the differential equations of equilibrium written in general orthogonal curvilinear coordinates have exactly been solved by means of the exponential matrix method. The 2D FE results have been obtained by means of the commercial finite element code MSC Nastran [8]. In the most general case of exact three-dimensional analyses, the number of frequencies for a free vibration problem is infinite: three displacement components (3 degrees of freedom DOF) in each point (points are ∞ in the 3 directions x, y, z) leads to $3 \times \infty^3$ vibration modes. Assumptions are made in the thickness direction z in the case of a two-dimensional plate/shell model, the three displacements in each point are expressed in terms of a given number of degrees of freedom (NDOF) through the thickness direction z . NDOF varies from theory to theory. As a result, the number of vibration modes is $NDOF \times \infty^2$ in the case of exact 2D models. For exact beam models, the number of vibration modes is $NDOF \times \infty^1$. In the case of computational models, such as the Finite Element (FE) method, the number of modes is a finite number. This number coincides with the number of employed degrees of freedom: $\sum_1^{Node} NDOF_i$, where $Node$ denotes the number of nodes used in the FE mathematical model, and $NDOF_i$ is the NDOF through the thickness direction z in the i -node. It is clear that some modes are tragically lost in simplified models (such as computational two-dimensional models) [4]. In order to make a comparison between the 2D FE free vibration results and the 3D exact free vibration results, the investigation of the vibration modes is mandatory in order to understand what are the frequencies that must be compared.

*Corresponding Author: Salvatore Brischetto: Salvatore Brischetto, Department of Mechanical and Aerospace Engineering, Politecnico di Torino, corso Duca degli Abruzzi, 24, 10129 Torino, ITALY. tel: +39.011.090.6813, fax: +39.011.090.6899, E-mail: salvatore.brischetto@polito.it.

Roberto Torre: Postgraduate at Politecnico di Torino

 © 2014 Salvatore Brischetto et al., licensee De Gruyter Open. This work is licensed under the Creative Commons Attribution-NonCommercial-NoDerivs 3.0 License.

The most relevant works about three-dimensional free vibration analysis of plates are shown below. Analytical three-dimensional solutions for free vibrations of a simply supported rectangular plate made of an incompressible homogeneous linear elastic isotropic material were proposed in Aimmanee and Batra [9] and in Batra and Aimmanee [10]. A three-dimensional linear elastic, small deformation theory obtained by the direct method was developed in Srinivas et al. [11] for the free vibration of simply supported, homogeneous, isotropic, thick rectangular plates. The same method was previously proposed in Srinivas et al. [12] for the flexure of simply supported homogeneous, isotropic, thick rectangular plates under arbitrary loads. Batra et al. [13] showed useful comparisons between two-dimensional models and an exact three-dimensional solution for free vibrations of a simply supported rectangular orthotropic thick plate. Ye [14] presented a three-dimensional elastic free vibration analysis of cross-ply laminated rectangular plates with clamped boundaries; the analysis was based on a recursive solution. Comparisons between 2D-displacement-based-models and exact results of the linear three-dimensional elasticity were proposed in Messina [15] for natural frequencies, displacement and stress quantities in multilayered plates. A global three-dimensional Ritz formulation was employed in Cheung and Zhou [16] for the exact three-dimensional elastic investigation of isosceles triangular plates, and in Liew and Yang [17] for the three-dimensional elastic free vibration analysis of a circular plate. A set of orthogonal polynomial series was used to approximate the spatial displacements. Theoretical high frequency vibration analysis is fundamental in a variety of engineering designs. The importance of high frequency analysis of multilayered composite plates was also confirmed in the literature [4]. Zhao et al. [18] introduced the discrete singular convolution (DSC) algorithm for high frequency vibration analysis of plate structures, the Levy method was also employed to provide exact solutions to validate the DSC algorithm. The same investigation (comparison between DSC algorithm and the Levy method) was also proposed in Wei et al. [19]. Taher et al. [20] computed the first nine frequency parameters of circular and annular plates with variable thickness and combined boundary conditions, the eigenvalue equation was derived by means of three-dimensional elasticity theory and Ritz method. Xing and Liu [21] proposed the separation of variables to solve the Hamiltonian dual form of eigenvalue problem for transverse free vibrations of thin plates. Vel and Batra [22] extended three-dimensional exact models to free vibration of functionally graded material plates.

The most relevant works about three-dimensional free vibration analysis of shells are shown below. The coupled free vibrations of a transversely isotropic cylindrical shell embedded in an elastic medium were studied in [23] where the three-dimensional elastic solution used three displacement functions to represent the three displacement components. Free vibrations of simply-supported cylindrical shells were studied in [24] on the basis of three dimensional exact theory. Extensive frequency parameters were obtained by solving frequency equations. The free vibrations of simply-supported cross-ply cylindrical and doubly-curved laminates were investigated in [25]. The three-dimensional equations of motion were reduced to a system of coupled ordinary differential equations and then solved using the power series method. The three-dimensional free vibrations of a homogenous isotropic, viscothermoelastic hollow sphere were studied in [26]. The surfaces were subjected to stress-free, thermally insulated or isothermal boundary conditions. The exact three-dimensional vibration analysis of a trans-radially isotropic, thermoelastic solid sphere was analyzed in [27]. The governing partial differential equations in [26] and [27] were transformed into a coupled system of ordinary differential equations. Fröbenius matrix method was employed to obtain the solution. Soldatos and Ye [28] proposed exact, three-dimensional, free vibration analysis of angle-ply laminated thick cylinders having a regular symmetric or a regular antisymmetric angle-ply lay-up. Armenakas et al. [29] proposed a self-contained treatment of the problem of plane harmonic waves propagation along a hollow circular cylinder in the framework of the three-dimensional theory of elasticity. A comparison between a refined two-dimensional analysis, a shear deformation theory, the Flügge theory and an exact elasticity analysis was proposed in [30] for frequency investigation. Further details about the Flügge classical thin shell theory concerning the free vibrations of cylindrical shells with elastic boundary conditions can be found in [31]. Other comparisons between two-dimensional closed form solutions and exact 3D elastic analytical solutions for the free vibration analysis of simply supported and clamped homogeneous isotropic circular cylindrical shells were also proposed in [32]. Vel [33] extended exact elasticity solutions to functionally graded cylindrical shells. The three-dimensional linear elastodynamics equations were solved using suitable displacement functions that identically satisfy the boundary conditions. Loy and Lam [34] obtained the governing equations using an energy minimization principle. A layer-wise approach was proposed to study the vibration of thick circular cylindrical shells on the basis of three-dimensional theory of elasticity. Wang et al. [35]

proposed the three-dimensional free vibration analysis of magneto-electro-elastic cylindrical panels. Further results about three-dimensional analysis of shells, where the solutions are not given in closed form, can be found in [36] for the dynamic stiffness matrix method and in [37] and [38] for the three-dimensional Ritz method for vibration of spherical shells.

The papers of the literature discussed in this introduction show the three-dimensional analysis for free vibrations of plates or shells. They separately analyze shell or plate geometries and they do not give a general overview for both structures. The proposed exact 3D model uses a general formulation for several geometries (square and rectangular plates, cylindrical and spherical shell panels, and cylindrical closed shells). The equations of motion for the dynamic case are written in general orthogonal curvilinear coordinates using an exact geometry for multilayered shells. The system of second order differential equations is reduced to a system of first order differential equations, and afterwards it is exactly solved using the exponential matrix method and the Navier-type solution. The approach is developed in layer-wise form imposing the continuity of displacements and transverse shear/normal stresses at each interface. The exponential matrix method has already been used in [15] for the three-dimensional analysis of plates in rectilinear orthogonal coordinates and in [28] for an exact, three-dimensional, free vibration analysis of angle-ply laminated cylinders in cylindrical coordinates. The equations of motion written in orthogonal curvilinear coordinates are a general form of the equations of motion written in rectilinear orthogonal coordinates in [15] and in cylindrical coordinates in [28]. The present equations allow general exact solutions for multilayered plate and shell geometries as already seen in the past author's works [5]-[7]. In the literature review proposed in this introduction, only few works analyzes higher order frequencies. Moreover, papers that discuss the comparison between 2D models and exact 3D models are even less. The present work aims to fill this gap, it proposes a comparison between the free frequencies for plates and cylinders obtained by means of the commercial FE code MSC NASTRAN and those obtained by means of the exact 3D solution. The proposed 3D exact solution gives results for plates, cylindrical and spherical shell panels, and cylindrical closed shells. However, the comparison with the commercial FE code is proposed only for plates and cylinders. This choice is made for the sake of brevity, and further investigations for cylindrical and spherical shell panels could be proposed in the future. The aim of the present paper is to understand how to compare these two

different methods (exact 3D and numerical 2D solutions) and also to show the limits of a classical 2D FE solution.

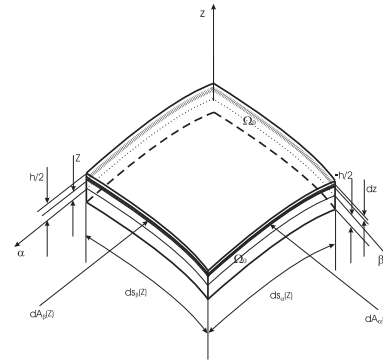


Figure 1: Geometry, notation and reference system for shells.

2 Exact elasticity solution for shells

The three differential equations of equilibrium written for the case of free vibration analysis of multilayered spherical shells made of N_L layers with constant radii of curvature R_α and R_β are (the general form for variable radii of curvature can be found in [39] and [40]):

$$H_\beta \frac{\partial \sigma_{\alpha\alpha k}}{\partial \alpha} + H_\alpha \frac{\partial \sigma_{\alpha\beta k}}{\partial \beta} + H_\alpha H_\beta \frac{\partial \sigma_{\alpha z k}}{\partial z} + \left(\frac{2H_\beta}{R_\alpha} + \frac{H_\alpha}{R_\beta} \right) \sigma_{\alpha z k} = \rho_k H_\alpha H_\beta \ddot{u}_k, \quad (1)$$

$$H_\beta \frac{\partial \sigma_{\alpha\beta k}}{\partial \alpha} + H_\alpha \frac{\partial \sigma_{\beta\beta k}}{\partial \beta} + H_\alpha H_\beta \frac{\partial \sigma_{\beta z k}}{\partial z} + \left(\frac{2H_\alpha}{R_\beta} + \frac{H_\beta}{R_\alpha} \right) \sigma_{\beta z k} = \rho_k H_\alpha H_\beta \ddot{v}_k, \quad (2)$$

$$H_\beta \frac{\partial \sigma_{\alpha z k}}{\partial \alpha} + H_\alpha \frac{\partial \sigma_{\beta z k}}{\partial \beta} + H_\alpha H_\beta \frac{\partial \sigma_{z z k}}{\partial z} - \frac{H_\beta}{R_\alpha} \sigma_{\alpha\alpha k} - \frac{H_\alpha}{R_\beta} \sigma_{\beta\beta k} + \left(\frac{H_\beta}{R_\alpha} + \frac{H_\alpha}{R_\beta} \right) \sigma_{z z k} = \rho_k H_\alpha H_\beta \ddot{w}_k, \quad (3)$$

where ρ_k is the mass density, $(\sigma_{\alpha\alpha k}, \sigma_{\beta\beta k}, \sigma_{z z k}, \sigma_{\beta z k}, \sigma_{\alpha z k}, \sigma_{\alpha\beta k})$ are the six stress components and \ddot{u}_k, \ddot{v}_k and \ddot{w}_k indicate the second temporal derivative of the three displacement components. Each quantity depends on the k layer. R_α and R_β are referred to the mid-surface Ω_0 of the whole multilayered shell (see Figure 1 for further details about shell geometry). H_α and H_β continuously vary through the thickness of the multilayered shell and they depend on the thickness coordinate. The parametric coefficients for

shells with constant radii of curvature are:

$$\begin{aligned}
 H_\alpha &= \left(1 + \frac{z}{R_\alpha}\right) = \left(1 + \frac{\tilde{z} - h/2}{R_\alpha}\right), \\
 H_\beta &= \left(1 + \frac{z}{R_\beta}\right) = \left(1 + \frac{\tilde{z} - h/2}{R_\beta}\right), \quad H_z = 1,
 \end{aligned}
 \tag{4}$$

H_α and H_β depend on z or \tilde{z} coordinate (see Figure 2 for further details).

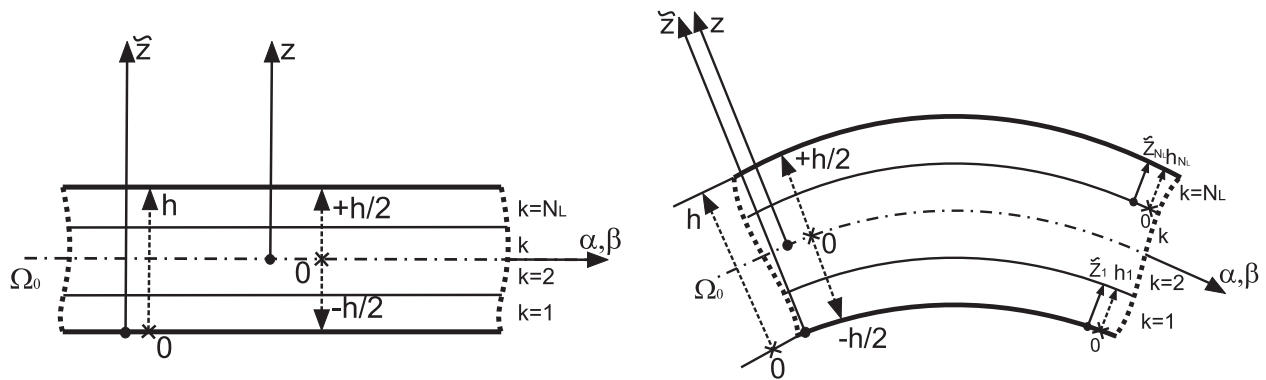


Figure 2: Thickness coordinates and reference systems for plates and shells.

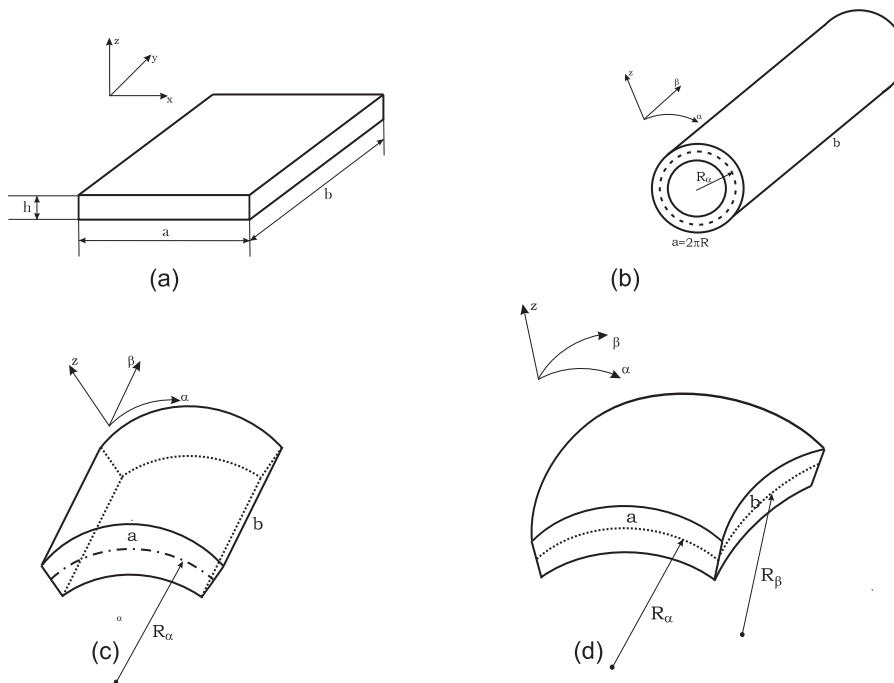


Figure 3: Geometries for assessments (structures a-d) and for benchmarks (structures a and b).

The geometrical relations written for shells with constant radii of curvature are obtained from the general strain-displacement relations of the three-dimensional theory of elasticity in orthogonal curvilinear coordinates proposed in [39] and [41]:

$$\epsilon_{\alpha\alpha k} = \frac{1}{H_\alpha} \frac{\partial u_k}{\partial \alpha} + \frac{w_k}{H_\alpha R_\alpha},
 \tag{5}$$

$$\epsilon_{\beta\beta k} = \frac{1}{H_\beta} \frac{\partial v_k}{\partial \beta} + \frac{w_k}{H_\beta R_\beta}, \quad (6)$$

$$\epsilon_{zzk} = \frac{\partial w_k}{\partial z}, \quad (7)$$

$$\gamma_{\alpha\beta k} = \frac{1}{H_\alpha} \frac{\partial v_k}{\partial \alpha} + \frac{1}{H_\beta} \frac{\partial u_k}{\partial \beta}, \quad (8)$$

$$\gamma_{\alpha z k} = \frac{1}{H_\alpha} \frac{\partial w_k}{\partial \alpha} + \frac{\partial u_k}{\partial z} - \frac{u_k}{H_\alpha R_\alpha}, \quad (9)$$

$$\gamma_{\beta z k} = \frac{1}{H_\beta} \frac{\partial w_k}{\partial \beta} + \frac{\partial v_k}{\partial z} - \frac{v_k}{H_\beta R_\beta}. \quad (10)$$

Geometrical relations for spherical shells degenerate into geometrical relations for cylindrical shells when R_α or R_β is infinite (with H_α or H_β equals one), and they degenerate into geometrical relations for plates when both R_α and R_β are infinite (with $H_\alpha=H_\beta=1$).

Three-dimensional linear elastic constitutive equations in orthogonal curvilinear coordinates (α, β, z) for orthotropic material in the structural reference system are given for a generic k layer of the multilayered structure:

$$\sigma_{\alpha\alpha k} = C_{11k}\epsilon_{\alpha\alpha k} + C_{12k}\epsilon_{\beta\beta k} + C_{13k}\epsilon_{zzk} + C_{16k}\gamma_{\alpha\beta k}, \quad (11)$$

$$\sigma_{\beta\beta k} = C_{12k}\epsilon_{\alpha\alpha k} + C_{22k}\epsilon_{\beta\beta k} + C_{23k}\epsilon_{zzk} + C_{26k}\gamma_{\alpha\beta k}, \quad (12)$$

$$\sigma_{zzk} = C_{13k}\epsilon_{\alpha\alpha k} + C_{23k}\epsilon_{\beta\beta k} + C_{33k}\epsilon_{zzk} + C_{36k}\gamma_{\alpha\beta k}, \quad (13)$$

$$\sigma_{\beta z k} = C_{44k}\gamma_{\beta z k} + C_{45k}\gamma_{\alpha z k}, \quad (14)$$

$$\sigma_{\alpha z k} = C_{45k}\gamma_{\beta z k} + C_{55k}\gamma_{\alpha z k}, \quad (15)$$

$$\sigma_{\alpha\beta k} = C_{16k}\epsilon_{\alpha\alpha k} + C_{26k}\epsilon_{\beta\beta k} + C_{36k}\epsilon_{zzk} + C_{66k}\gamma_{\alpha\beta k}. \quad (16)$$

The closed form of Eqs. (1)-(3) is obtained for simply supported shells and plates made of isotropic material or orthotropic material with 0° or 90° orthotropic angle (in both cases $C_{16k} = C_{26k} = C_{36k} = C_{45k} = 0$). The three displacement components have the following harmonic form:

$$u_k(\alpha, \beta, z, t) = U_k(z)e^{i\omega t} \cos(\bar{\alpha}\alpha) \sin(\bar{\beta}\beta), \quad (17)$$

$$v_k(\alpha, \beta, z, t) = V_k(z)e^{i\omega t} \sin(\bar{\alpha}\alpha) \cos(\bar{\beta}\beta), \quad (18)$$

$$w_k(\alpha, \beta, z, t) = W_k(z)e^{i\omega t} \sin(\bar{\alpha}\alpha) \sin(\bar{\beta}\beta), \quad (19)$$

where U_k , V_k and W_k are the displacement amplitudes in α , β and z directions, respectively. i is the coefficient of the imaginary unit, $\omega = 2\pi f$ is the circular frequency where f is the frequency value, t is the time. In coefficients $\bar{\alpha} = \frac{m\pi}{a}$ and $\bar{\beta} = \frac{n\pi}{b}$, m and n are the half-wave numbers and a and b are the shell dimensions in α and β directions, respectively (calculated in the mid-surface Ω_0).

The system of equations in closed form is obtained substituting Eqs. (5)-(10), (11)-(16) and (17)-(19) in the equilibrium equations proposed in Eqs. (1)-(3):

$$\begin{aligned} & \left(-\frac{C_{55k}H_\beta}{H_\alpha R_\alpha^2} - \frac{C_{55k}}{R_\alpha R_\beta} - \bar{\alpha}^2 \frac{C_{11k}H_\beta}{H_\alpha} - \bar{\beta}^2 \frac{C_{66k}H_\alpha}{H_\beta} + \rho_k H_\alpha H_\beta \omega^2 \right) U_k + \left(-\bar{\alpha}\bar{\beta}C_{12k} - \bar{\alpha}\bar{\beta}C_{66k} \right) V_k + \\ & \left(\bar{\alpha} \frac{C_{11k}H_\beta}{H_\alpha R_\alpha} + \bar{\alpha} \frac{C_{12k}}{R_\beta} + \bar{\alpha} \frac{C_{55k}H_\beta}{H_\alpha R_\alpha} + \bar{\alpha} \frac{C_{55k}}{R_\beta} \right) W_k + \left(\frac{C_{55k}H_\beta}{R_\alpha} + \frac{C_{55k}H_\alpha}{R_\beta} \right) U_{k,z} + \left(\bar{\alpha}C_{13k}H_\beta + \right. \\ & \left. \bar{\alpha}C_{55k}H_\beta \right) W_{k,z} + \left(C_{55k}H_\alpha H_\beta \right) U_{k,zz} = 0, \end{aligned} \quad (20)$$

$$\begin{aligned} & \left(-\bar{\alpha}\bar{\beta}C_{66k} - \bar{\alpha}\bar{\beta}C_{12k} \right) U_k + \left(-\frac{C_{44k}H_\alpha}{H_\beta R_\beta^2} - \frac{C_{44k}}{R_\alpha R_\beta} - \bar{\alpha}^2 \frac{C_{66k}H_\beta}{H_\alpha} - \bar{\beta}^2 \frac{C_{22k}H_\alpha}{H_\beta} + \rho_k H_\alpha H_\beta \omega^2 \right) V_k + \\ & \left(\bar{\beta} \frac{C_{44k}H_\alpha}{H_\beta R_\beta} + \bar{\beta} \frac{C_{44k}}{R_\alpha} + \bar{\beta} \frac{C_{22k}H_\alpha}{H_\beta R_\beta} + \bar{\beta} \frac{C_{12k}}{R_\alpha} \right) W_k + \left(\frac{C_{44k}H_\alpha}{R_\beta} + \frac{C_{44k}H_\beta}{R_\alpha} \right) V_{k,z} + \left(\bar{\beta}C_{44k}H_\alpha + \right. \\ & \left. \bar{\beta}C_{23k}H_\alpha \right) W_{k,z} + \left(C_{44k}H_\alpha H_\beta \right) V_{k,zz} = 0, \\ & \left(\bar{\alpha} \frac{C_{55k}H_\beta}{H_\alpha R_\alpha} - \bar{\alpha} \frac{C_{13k}}{R_\beta} + \bar{\alpha} \frac{C_{11k}H_\beta}{H_\alpha R_\alpha} + \bar{\alpha} \frac{C_{12k}}{R_\beta} \right) U_k + \left(\bar{\beta} \frac{C_{44k}H_\alpha}{H_\beta R_\beta} - \bar{\beta} \frac{C_{23k}}{R_\alpha} + \bar{\beta} \frac{C_{22k}H_\alpha}{H_\beta R_\beta} + \bar{\beta} \frac{C_{12k}}{R_\alpha} \right) V_k + \end{aligned} \quad (21)$$

$$\begin{aligned}
& \left(\frac{C_{13k}}{R_\alpha R_\beta} + \frac{C_{23k}}{R_\alpha R_\beta} - \frac{C_{11k} H_\beta}{H_\alpha R_\alpha^2} - \frac{2C_{12k}}{R_\alpha R_\beta} - \frac{C_{22k} H_\alpha}{H_\beta R_\beta^2} - \bar{\alpha}^2 \frac{C_{55k} H_\beta}{H_\alpha} - \bar{\beta}^2 \frac{C_{44k} H_\alpha}{H_\beta} + \rho_k H_\alpha H_\beta \omega^2 \right) W_k + \\
& \left(-\bar{\alpha} C_{55k} H_\beta - \bar{\alpha} C_{13k} H_\beta \right) U_{k,z} + \left(-\bar{\beta} C_{44k} H_\alpha - \bar{\beta} C_{23k} H_\alpha \right) V_{k,z} + \left(\frac{C_{33k} H_\beta}{R_\alpha} + \frac{C_{33k} H_\alpha}{R_\beta} \right) W_{k,z} + \\
& \left(C_{33k} H_\alpha H_\beta \right) W_{k,zz} = 0.
\end{aligned} \tag{22}$$

The system of Eqs. (20)-(22) can be written in a compact form introducing coefficients A_{sk} for each block $(\)$ with s from 1 to 19:

$$A_{1k} U_k + A_{2k} V_k + A_{3k} W_k + A_{4k} U_{k,z} + A_{5k} W_{k,z} + A_{6k} U_{k,zz} = 0, \tag{23}$$

$$A_{7k} U_k + A_{8k} V_k + A_{9k} W_k + A_{10k} V_{k,z} + A_{11k} W_{k,z} + A_{12k} V_{k,zz} = 0, \tag{24}$$

$$A_{13k} U_k + A_{14k} V_k + A_{15k} W_k + A_{16k} U_{k,z} + A_{17k} V_{k,z} + A_{18k} W_{k,z} + A_{19k} W_{k,zz} = 0. \tag{25}$$

The Eqs. (23)-(25) are a system of three second order differential equations. They are written for spherical shell panels with constant radii of curvature but they automatically degenerate into equations for cylindrical shells and plates.

The system of second order differential equations proposed in Eqs. (23)-(25) can be reduced to a system of first order differential equations using the method described in [42] and [43] (further details can also be found in past author's works [5–7]):

$$\begin{bmatrix} A_{6k} & 0 & 0 & 0 & 0 & 0 \\ 0 & A_{12k} & 0 & 0 & 0 & 0 \\ 0 & 0 & A_{19k} & 0 & 0 & 0 \\ 0 & 0 & 0 & A_{6k} & 0 & 0 \\ 0 & 0 & 0 & 0 & A_{12k} & 0 \\ 0 & 0 & 0 & 0 & 0 & A_{19k} \end{bmatrix} \begin{bmatrix} U_k \\ V_k \\ W_k \\ U'_k \\ V'_k \\ W'_k \end{bmatrix}' = \begin{bmatrix} 0 & 0 & 0 & A_{6k} & 0 & 0 \\ 0 & 0 & 0 & 0 & A_{12k} & 0 \\ 0 & 0 & 0 & 0 & 0 & A_{19k} \\ -A_{1k} & -A_{2k} & -A_{3k} & -A_{4k} & 0 & -A_{5k} \\ -A_{7k} & -A_{8k} & -A_{9k} & 0 & -A_{10k} & -A_{11k} \\ -A_{13k} & -A_{14k} & -A_{15k} & -A_{16k} & -A_{17k} & -A_{18k} \end{bmatrix} \begin{bmatrix} U_k \\ V_k \\ W_k \\ U'_k \\ V'_k \\ W'_k \end{bmatrix}. \tag{26}$$

Eq. (26) can be written in a compact form for a generic k layer:

$$\mathbf{D}_k \frac{\partial \mathbf{U}_k}{\partial \tilde{z}} = \mathbf{A}_k \mathbf{U}_k, \tag{27}$$

where $\frac{\partial \mathbf{U}_k}{\partial \tilde{z}} = \mathbf{U}'_k$ and $\mathbf{U}_k = [U_k \ V_k \ W_k \ U'_k \ V'_k \ W'_k]$. The Eq. (27) can be written as:

$$\mathbf{D}_k \mathbf{U}'_k = \mathbf{A}_k \mathbf{U}_k, \tag{28}$$

$$\mathbf{U}'_k = \mathbf{D}_k^{-1} \mathbf{A}_k \mathbf{U}_k, \tag{29}$$

$$\mathbf{U}'_k = \mathbf{A}_k^* \mathbf{U}_k, \tag{30}$$

with $\mathbf{A}_k^* = \mathbf{D}_k^{-1} \mathbf{A}_k$.

In the case of plate geometry coefficients A_{3k} , A_{4k} , A_{9k} , A_{10k} , A_{13k} , A_{14k} and A_{18k} are zero because the radii of curvature R_α and R_β are infinite. The other coefficients A_{1k} , A_{2k} , A_{5k} , A_{6k} , A_{7k} , A_{8k} , A_{11k} , A_{12k} , A_{15k} , A_{16k} , A_{17k} and A_{19k} are constant in each k layer because parametric coefficients $H_\alpha = H_\beta = 1$ and they do not depend on the thickness coordinate \tilde{z} . Therefore, matrices \mathbf{D}_k , \mathbf{A}_k and \mathbf{A}_k^* are constant in each k layer of the plate. The solution of Eq. (30) for the plate case can be written as [43], [44]:

$$\mathbf{U}_k(\tilde{z}_k) = \exp(\mathbf{A}_k^* \tilde{z}_k) \mathbf{U}_k(0) \quad \text{with } \tilde{z}_k \in [0, h_k], \tag{31}$$

where \tilde{z}_k is the thickness coordinate of each layer from 0 at the bottom to h_k at the top (see Figure 2). The exponential matrix for the plate case (constant coefficients A_{sk}) is calculated with $\tilde{z}_k = h_k$ for each k layer as:

$$\mathbf{A}_k^{**} = \exp(\mathbf{A}_k^* h_k) = \mathbf{I} + \mathbf{A}_k^* h_k + \frac{\mathbf{A}_k^{*2}}{2!} h_k^2 + \frac{\mathbf{A}_k^{*3}}{3!} h_k^3 + \dots + \frac{\mathbf{A}_k^{*N}}{N!} h_k^N, \tag{32}$$

where \mathbf{I} is the 6×6 identity matrix. This expansion has a fast convergence as indicated in [45] and it is not time consuming from the computational point of view. In the case of N_L layers for shell geometry \mathbf{A}_k^* is not constant in each k layer because $H_\alpha(\tilde{z})$ and $H_\beta(\tilde{z})$ are not constant.

In the case of multilayered plates, $N_L - 1$ transfer matrices $\mathbf{T}_{k-1,k}$ must be calculated using for each interface the following conditions for interlaminar continuity of displacements and transverse shear/normal stresses:

$$u_k^b = u_{k-1}^t, \quad v_k^b = v_{k-1}^t, \quad w_k^b = w_{k-1}^t, \tag{33}$$

$$\sigma_{zzk}^b = \sigma_{zzk-1}^t, \quad \sigma_{\alpha zk}^b = \sigma_{\alpha zk-1}^t, \quad \sigma_{\beta zk}^b = \sigma_{\beta zk-1}^t, \tag{34}$$

each displacement and transverse stress component at the top (t) of the $k-1$ layer is equal to displacement and transverse stress components at the bottom (b) of the k layer.

The Eqs. (33)-(34) can be grouped in a system (details can be found in [5], [6] and [7]):

$$\begin{bmatrix} U \\ V \\ W \\ U' \\ V' \\ W' \end{bmatrix}_k^b = \begin{bmatrix} 1 & 0 & 0 & 0 & 0 & 0 \\ 0 & 1 & 0 & 0 & 0 & 0 \\ 0 & 0 & 1 & 0 & 0 & 0 \\ T_1 & 0 & T_2 & T_3 & 0 & 0 \\ 0 & T_4 & T_5 & 0 & T_6 & 0 \\ T_7 & T_8 & T_9 & 0 & 0 & T_{10} \end{bmatrix}_{k-1,k} \begin{bmatrix} U \\ V \\ W \\ U' \\ V' \\ W' \end{bmatrix}_{k-1}^t, \tag{35}$$

Eq. (35) in compact form is:

$$\mathbf{U}_k^b = \mathbf{T}_{k-1,k} \mathbf{U}_{k-1}^t. \tag{36}$$

The calculated $\mathbf{T}_{k-1,k}$ matrices allow to link \mathbf{U} at the bottom (b) of the k layer with \mathbf{U} at the top (t) of the $k - 1$ layer. Eq. (36) can also be written as:

$$\mathbf{U}_k(0) = \mathbf{T}_{k-1,k} \mathbf{U}_{k-1}(h_{k-1}), \tag{37}$$

where \mathbf{U}_k is calculated for $\tilde{z}_k = 0$ and \mathbf{U}_{k-1} is calculated for $\tilde{z}_{k-1} = h_{k-1}$. \mathbf{U} at the top of the k layer is linked with \mathbf{U} at the bottom of the same k layer by means of the exponential matrix \mathbf{A}_k^{**} :

$$\mathbf{U}_k(h_k) = \mathbf{A}_k^{**} \mathbf{U}_k(0), \tag{38}$$

Eq. (37) can recursively be introduced in Eq. (38) for the $N_L - 1$ interfaces to obtain:

$$\mathbf{U}_{N_L}(h_{N_L}) = \mathbf{A}_{N_L}^{**} \mathbf{T}_{N_L-1,N_L} \mathbf{A}_{N_L-1}^{**} \mathbf{T}_{N_L-2,N_L-1} \dots \mathbf{A}_2^{**} \mathbf{T}_{1,2} \mathbf{A}_1^{**} \mathbf{U}_1(0), \tag{39}$$

the definition of the matrix \mathbf{H}_m for the multilayered plate allows Eq. (39) to be written as:

$$\mathbf{U}_{N_L}(h_{N_L}) = \mathbf{H}_m \mathbf{U}_1(0), \tag{40}$$

that links \mathbf{U} calculated at the top of the last N_L layer with \mathbf{U} calculated at the bottom of the first layer. In the case of multilayered plates, matrices \mathbf{D}_k , \mathbf{A}_k and \mathbf{A}_k^* are constant in each k layer because R_α and R_β are infinite and H_α and H_β equal 1. In the case of shell geometry matrices \mathbf{D}_k , \mathbf{A}_k and \mathbf{A}_k^* are not constant in each layer because of parametric coefficients H_α and H_β that depend on \tilde{z} coordinate (see Figure 2). A first method could be the use of hypothesis $\frac{z}{R_\alpha} = \frac{z}{R_\beta} = 0$ (it is valid only for very thin shells) that means $H_\alpha = H_\beta = 1$. In this case the solution is the same already seen for the multilayered plate because matrices \mathbf{D}_k , \mathbf{A}_k and \mathbf{A}_k^* are constant in each k layer. This method is not used in this paper because it is an approximation that is valid only for very thin shells, and it does not consider the exact geometry of the structure. The second method (used in this paper) is the introduction of several j fictitious layers in each k physical layer where H_α and H_β can exactly be calculated. Matrices \mathbf{A}_j^{**} are constant in the j layer because they are evaluated with R_α , R_β , $\bar{\alpha}$ and $\bar{\beta}$ calculated in the mid-surface Ω_0 of the whole shell, and with H_α and H_β calculated in the middle of each j fictitious layer. Matrices $\mathbf{T}_{j-1,j}$ are also constant because they are calculated with R_α , R_β , $\bar{\alpha}$ and $\bar{\beta}$ calculated in the mid-surface Ω_0 of the shell, and with H_α and H_β calculated at each fictitious interface. In the present paper each physical k layer of the multilayered shell is divided in j fictitious layers where we can recursively apply the Eqs. (36)-(40) with index $q=k \times j$ in place of index k . The thickness of each fictitious layer is h_q . The index q considers all the fictitious and physical layers and it goes from 1 to P . $N=3$ for the exponential matrix in Eq. (32) for each q layer guarantees the exact convergence for each shell investigated. The total number of mathematical layers that will be used for multilayered shell investigations will be $P=102$ or $P=100$ (it will depend on the analyzed case).

The structures are simply supported and free stresses at the top and at the bottom of the whole multilayered shell, this feature means:

$$\sigma_{zz} = \sigma_{az} = \sigma_{\beta z} = 0 \quad \text{for } z = -h/2, +h/2 \quad \text{or } \tilde{z} = 0, h, \quad (41)$$

$$w = v = 0, \quad \sigma_{\alpha\alpha} = 0 \quad \text{for } \alpha = 0, a, \quad (42)$$

$$w = u = 0, \quad \sigma_{\beta\beta} = 0 \quad \text{for } \beta = 0, b. \quad (43)$$

Eqs. (41)-(43) in compact form to express the free stress state at the top and bottom of the whole shell are (further details can be found in [5], [6] and [7]):

$$\mathbf{B}_P(h_P) \mathbf{U}_P(h_P) = \mathbf{0}, \quad (44)$$

$$\mathbf{B}_1(0) \mathbf{U}_1(0) = \mathbf{0}, \quad (45)$$

Eq. (40) can be substituted in Eq. (44) considering a total number of layers equals P (both physical and fictitious layers, and not only the physical layers N_L):

$$\mathbf{B}_P(h_P) \mathbf{H}_m \mathbf{U}_1(0) = \mathbf{0}, \quad (46)$$

$$\mathbf{B}_1(0) \mathbf{U}_1(0) = \mathbf{0}, \quad (47)$$

Eqs. (46) and (47) can be grouped in the following system:

$$\begin{bmatrix} \mathbf{B}_P(h_P) \mathbf{H}_m \\ \mathbf{B}_1(0) \end{bmatrix} \mathbf{U}_1(0) = \mathbf{0}, \quad (48)$$

and introducing the 6×6 \mathbf{E} matrix, the Eq. (48) is:

$$\mathbf{E} \mathbf{U}_1(0) = \mathbf{0}. \quad (49)$$

The Eq. (49) is also valid for plate case where the fictitious layers are not introduced and $\mathbf{B}_{N_L}(h_{N_L}) = \mathbf{B}_P(h_P)$. Matrix \mathbf{E} has always 6×6 dimension, independently from the number of layers P, even if the method uses a layer-wise approach. The solution is implemented in a Matlab code where only the spherical shell method is considered, it automatically degenerates into cylindrical open/closed shell and plate geometries.

The free vibration analysis means to find the non-trivial solution of $\mathbf{U}_1(0)$ in Eq. (49), this means to impose the determinant of matrix \mathbf{E} equals zero:

$$\det[\mathbf{E}] = 0, \quad (50)$$

Eq. (50) means to find the roots of an higher order polynomial in $\lambda = \omega^2$. For each pair of half-wave numbers (m,n) a certain number of circular frequencies are obtained depending on the order N chosen for each exponential matrix \mathbf{A}_q^{**} .

A certain number of circular frequencies ω_l are found when half-wave numbers m and n are imposed in the structures. For each frequency ω_l , it is possible to find the vibration mode through the thickness in terms of the three displacement components. If the frequency ω_l is substituted

in the 6×6 matrix \mathbf{E} , this last matrix has six eigenvalues. We are interested to the null space of matrix \mathbf{E} that means to find the 6×1 eigenvector related to the minimum of the six eigenvalues proposed. This null space is, for the chosen frequency ω_l , the vector \mathbf{U} calculated at the bottom of the whole structure:

$$\begin{aligned} \mathbf{U}_{1\omega_l}(0) &= \\ &= \begin{bmatrix} U_1(0) & V_1(0) & W_1(0) & U'_1(0) & V'_1(0) & W'_1(0) \end{bmatrix}_{\omega_l}^T, \end{aligned} \quad (51)$$

T means the transpose of the vector and the subscript ω_l means that the null space is calculated for the circular frequency ω_l .

It is possible to find $\mathbf{U}_{q\omega_l}(\tilde{z}_q)$ (with the three displacement components $U_{q\omega_l}(\tilde{z}_q)$, $V_{q\omega_l}(\tilde{z}_q)$ and $W_{q\omega_l}(\tilde{z}_q)$ through the thickness) for each q layer of the multilayered structure using Eqs. (37)-(40) with the index q (in place of k) from 1 to P. The thickness coordinate \tilde{z} can assume all the values from the bottom to the top of the structure. For the plate case the procedure is simpler because there are not the j fictitious layers and the index q coincides with the index k of the physical layers (in this case, the total number of layers is N_L and it is not P).

2.1 Validation of the 3D exact model

Before the comparison study between the 3D exact solution and the 2D FE solution, the proposed 3D exact model has been validated by means of several comparisons with other 3D results already given in the literature. The validation considers plates, cylinders, cylindrical panels and spherical panels (see Figure 3 for further details). Both one-layered and multilayered configurations are analyzed. The order of expansion employed for the exponential matrix is $N=3$. $P=100$ fictitious layers have been used for the investigation of one-, two- and four-layered structures. $P=102$ fictitious layers have been used for the investigation of three-layered structures. An appropriate convergence study has already been proposed in [5], [6] and [7].

The first assessment considers a simply supported one-layered square plate ($a=b=10$ m) with thickness $h=1$ m. The only embedded layer is the isotropic aluminium alloy with Young modulus $E=70$ GPa, Poisson ratio $\nu=0.3$ and mass density $\rho=2702$ kg/m³. The first six circular frequencies are given in non-dimensional form $\tilde{\omega} = \omega \frac{a^2}{h} \sqrt{\frac{\rho}{E}}$ for half-wave numbers $m=n=1$. Table 1 compares the present 3D solution with 3D solutions by Vel and Batra [22] and Srinivas et al. [12]. Compared results are identical for each proposed vibration mode.

Table 1: First assessment for the 3D exact solution, simply supported plate made of aluminium alloy with thickness ratio $a/h=10$. First six circular frequencies $\bar{\omega} = \omega \frac{a^2}{h} \sqrt{\frac{\rho}{E}}$ for half-wave numbers $m=n=1$.

Mode	I	II	III	IV	V	VI
3D [22]	5.7769	27.554	46.503	196.77	201.34	357.42
3D [12]	5.7769	27.554	46.503	196.77	201.34	357.42
Present 3D	5.7769	27.554	46.502	196.77	201.34	357.42

The second assessment shows the free frequencies for a simply supported one-layered cylinder with radii of curvature $R_\alpha=1$ m and $R_\beta = \infty$, and circular dimension $a = 2\pi R_\alpha$. The material is isotropic (the same aluminium alloy proposed in the first assessment). In Table 2, the proposed thickness values are $h=0.12$ m and $h=0.18$ m, and the b dimension values can be 2m or 1 m. Table 2 shows the first circular frequency in non-dimensional form $\bar{\omega} = \omega \frac{h}{\pi} \sqrt{\frac{\rho}{G}}$ for longitudinal half-wave number $n=1$ and several m circular half-wave numbers. The present 3D solution is coincident with 3D solutions by Armenakas et al. [29] and Bhimaraddi [30] for each proposed h/R_α and b/R_α ratios.

Table 2: Second assessment for the 3D exact solution, simply supported cylinder made of aluminium alloy with different thickness ratios h/R_α . First circular frequency $\bar{\omega} = \omega \frac{h}{\pi} \sqrt{\frac{\rho}{G}}$ for $n=1$ and several m values.

$h/R_\alpha = 0.12$				
m	2	4	6	8
$b/R_\alpha = 2$				
3D [29, 30]	0.03730	0.02359	0.02462	0.03686
Present 3D	0.03730	0.02359	0.02462	0.03686
$b/R_\alpha = 1$				
3D [29, 30]	0.05853	0.04978	0.04789	0.05545
Present 3D	0.05853	0.04978	0.04789	0.05545
$h/R_\alpha = 0.18$				
m	2	4	6	8
$b/R_\alpha = 2$				
3D [29, 30]	0.05652	0.03929	0.04996	0.07821
Present 3D	0.05652	0.03929	0.04996	0.07821
$b/R_\alpha = 1$				
3D [29, 30]	0.09402	0.08545	0.09093	0.11205
Present 3D	0.09402	0.08545	0.09093	0.11205

The third assessment gives several frequencies for a simply supported multilayered composite cylindrical panel with radii of curvature $R_\alpha=10$ m and $R_\beta = \infty$, and dimensions $a=b=5$ m. The thickness is $h=0.5$ m (the shell is moderately thick with a thickness ratio $R_\alpha/h=20$). The composite layers have properties $E_1 = 25E_0$, $E_2 = E_3 = E_0$,

$G_{12} = G_{13} = 0.5E_0$, $G_{23} = 0.2E_0$, $\nu_{12} = \nu_{13} = \nu_{23} = 0.25$ and $\rho = 1500 \text{ kg/m}^3$. Non-dimensional circular frequencies $\bar{\omega} = \omega R_\alpha \sqrt{\frac{\rho}{E_0}}$ for several physical layers N_L and lamination sequence ($0^\circ/90^\circ/0^\circ/90^\circ/\dots$) are given in Table 3. The imposed half-wave numbers m and n are indicated in the table. For $m=n=1$ the first three modes are shown, only the first mode is given for the other combinations of half-wave numbers m and n . The present 3D solution is coincident with the 3D solution by Huang [25] for each proposed half-wave number, vibration mode, and number of physical layers N_L embedded in the multilayered composite structure.

The last assessment considers several frequencies for a simply supported multilayered composite spherical panel with radii of curvature $R_\alpha=10$ m and $R_\beta=10$ m, dimensions $a=b=2$ m and thickness value $h=0.2$ m (the shell is moderately thin with a thickness ratio $R_\alpha/h=50$). The composite layers have the same properties already seen for the third assessment. Non-dimensional circular frequencies $\bar{\omega} = \omega R_\alpha \sqrt{\frac{\rho}{E_0}}$ for several physical layers N_L and lamination sequence ($0^\circ/90^\circ/0^\circ/90^\circ/\dots$) are given in Table 4. The present 3D solution gives the same results of the 3D solution by Huang [25] for each proposed half-wave number and for each number of physical layers N_L embedded in the multilayered composite structure. The first vibration mode is investigated for each combination of half-wave numbers m and n .

The proposed 3D solution has successfully been validated for each geometry (plate, cylinder, cylindrical and spherical shell panels), lamination sequence, embedded material, thickness ratio, vibration mode and imposed half-wave numbers. Therefore, it can be used with confidence to validate the FE models and also to make the comparisons between the exact 3D solutions and the computational 2D models.

3 Finite element model

The 2D finite element results proposed in this paper have been obtained by means of the FE commercial code known

Table 3: Third assessment for the 3D exact solution, simply supported composite cylindrical panel with thickness ratio $R_\alpha/h = 20$. Circular frequencies $\bar{\omega} = \omega R_\alpha \sqrt{\frac{\rho}{E_0}}$ for several physical layers N_L , lamination sequence ($0^\circ/90^\circ/0^\circ/90^\circ/\dots$) and half-wave numbers m and n .

m,n	mode	$N_L = 2$		$N_L = 4$		$N_L = 10$	
		3D [25]	Present 3D	3D [25]	Present 3D	3D [25]	Present 3D
1,1	I	1.8971	1.8971	2.3415	2.3415	2.4930	2.4930
1,1	II	18.813	18.813	21.545	21.545	22.387	22.387
1,1	III	20.169	20.169	22.902	22.902	23.694	23.694
1,2	I	4.4492	4.4492	4.9620	4.9620	5.3017	5.3017
1,3	I	7.8195	7.8195	8.0752	8.0753	8.5254	8.5253
2,1	I	4.3485	4.3485	4.8493	4.8493	5.1853	5.1853
2,2	I	6.0384	6.0384	6.5486	6.5486	6.9739	6.9739
2,3	I	8.8895	8.8895	9.1438	9.1438	9.6347	9.6346
3,1	I	7.7503	7.7503	7.9573	7.9573	8.3952	8.3950
3,2	I	8.9012	8.9012	9.1290	9.1290	9.6122	9.6120
3,3	I	11.103	11.103	11.164	11.164	11.686	11.686

Table 4: Fourth assessment for the 3D exact solution, simply supported composite spherical panel with thickness ratio $R_\alpha/h = 50$. Circular frequencies $\bar{\omega} = \omega R_\alpha \sqrt{\frac{\rho}{E_0}}$ for several physical layers N_L , lamination sequence ($0^\circ/90^\circ/0^\circ/90^\circ/\dots$) and half-wave numbers m and n .

m,n	mode	$N_L = 2$		$N_L = 4$		$N_L = 10$	
		3D [25]	Present 3D	3D [25]	Present 3D	3D [25]	Present 3D
1,1	I	4.6238	4.6240	5.8070	5.8070	6.2293	6.2293
1,2	I	10.753	10.753	12.134	12.134	13.050	13.050
1,3	I	19.130	19.130	19.846	19.845	21.042	21.042
2,1	I	10.864	10.864	12.188	12.188	13.076	13.076
2,2	I	14.909	14.909	16.298	16.298	17.432	17.432
2,3	I	21.961	21.961	22.719	22.719	24.027	24.027
3,1	I	19.315	19.315	19.932	19.931	21.082	21.081
3,2	I	22.053	22.053	22.757	22.757	24.045	24.045
3,3	I	27.483	27.483	27.790	27.790	29.189	29.189

as MSC Nastran & Patran [8]. Only simple geometries are analyzed in this paper (plates and cylinders). For these structures a maximum number of 5000 elements is sufficient for a correct convergence in the case of free vibration analysis (as it will be demonstrated in the section about the validation of the FE model). The 2D element employed in the free vibration analysis is the SHELL QUAD4 element of Nastran, it has four nodes for each element that are collocated in the four corners. The kinematic model used by Nastran in its 2D FEs is based on the Reissner-Mindlin hypotheses (equivalent single layer approach and constant transverse displacement in the z direction).

3.1 Validation of the 2D FE model

The FE model will be validated only for plates and cylinders because in Section 4 comparisons will be made only

for these two geometries. This choice is due to the fact that we want to compare several laminations, materials and modes without lose in clarity and conciseness. The investigation for cylindrical and spherical panels could be the topic of a future work.

The first assessment for the FE model considers a simply supported one-layered square plate (dimensions $a=b=1$ m) with thickness ratios $a/h=1000$ and $a/h=100$. The layer is made of an isotropic aluminium alloy with Young modulus $E=73$ GPa, Poisson ratio $\nu=0.3$ and mass density $\rho = 2800$ kg/m³. The second assessment for the FE model analyzes a simply supported two-layered cylinder (radii of curvature $R_\alpha=10$ m and $R_\beta=\infty$, and dimensions $a = 2\pi R_\alpha$ and $b=20$ m) with thickness ratios $R_\alpha/h=1000$ and $R_\alpha/h=100$. The isotropic layer at the bottom is the same already seen for the first assessment about the one-layered isotropic plate. The isotropic layer at the top is a titanium alloy with Young modulus $E=114$ GPa, Poisson

ratio $\nu=0.3$ and mass density $\rho = 2768\text{kg/m}^3$. The third assessment for the FE model proposes the same geometry of the cylinder described in the second assessment. In this third case, the structure is simply supported and it is multilayered embedding three composite layers with lamination sequence $90^\circ/0^\circ/90^\circ$. The composite material has Young moduli $E_1=132.38\text{ GPa}$ and $E_2=E_3=10.756\text{ GPa}$, shear moduli $G_{12}=G_{13}=5.6537\text{ GPa}$ and $G_{23}=3.603\text{ GPa}$, Poisson ratios $\nu_{12}=\nu_{13}=0.24$ and $\nu_{23}=0.49$, and mass density $\rho = 1600\text{ kg/m}^3$. In each table and figure, the first two frequencies obtained via the FE code are shown. The frequency values are given in Hz.

The results for the first assessment are shown in Table 5. For both thickness ratios ($a/h=1000$ and $a/h=100$), the first frequency is obtained with imposed half-wave numbers $m=n=1$, and the second frequency is obtained with $m=1$ and $n=2$. FE results with a rare mesh are more rigid than 3D results, therefore frequency values are bigger. These frequency values decrease and they are coincident with the 3D exact results when the mesh size increases. For a 70×70 mesh (that means 4900 elements), the FE value is very close to the 3D exact value for both frequencies (first and second) and for both thickness ratios ($a/h=1000$ and $a/h=100$). The error in percentage $\Delta(\%)$ is always less than 0.1%. Results of Table 5 are also shown in graphical form in Figures 4 and 5 for $a/h=1000$ and $a/h=100$, respectively. The top image is for the first frequency and the bottom image is for the second frequency.

The results for the second assessment are shown in Table 6. The structure is two-layered with a transverse anisotropy, the FE results converge to the 3D exact solution when the mesh size increases. For the cylinder with $R_\alpha/h=1000$, the first frequency is obtained with circular half-wave number $m=18$ and longitudinal half-wave number $n=1$, the second frequency is obtained with $m=20$ and $n=1$. For the thicker cylinder ($R_\alpha/h=100$), the first frequency is for $m=10$ and $n=1$, and the second frequency is for $m=12$ and $n=1$. For a rare mesh, the error given by the 2D FE model is large, this error is almost zero for a refinement of the mesh (127×38 that means 4826 elements). These results are confirmed in graphical form in Figures 6 and 7 for thickness ratios $R_\alpha/h=1000$ and $R_\alpha/h=100$, respectively. In this assessment, 2D frequencies are sometimes smaller than 3D frequencies. However, these differences are negligible (always less than $|0.1|\%$).

The third assessment is a composite three-layered cylinder, it is shown in Table 7. The first frequency is obtained with $m=22$ and $n=1$ for thickness ratio $R_\alpha/h=1000$, and with $m=12$ and $n=1$ for $R_\alpha/h=100$. The second frequency is obtained with $m=24$ and $n=1$ for thickness ratio $R_\alpha/h=1000$, and with $m=10$ and $n=1$ for $R_\alpha/h=100$. 2D

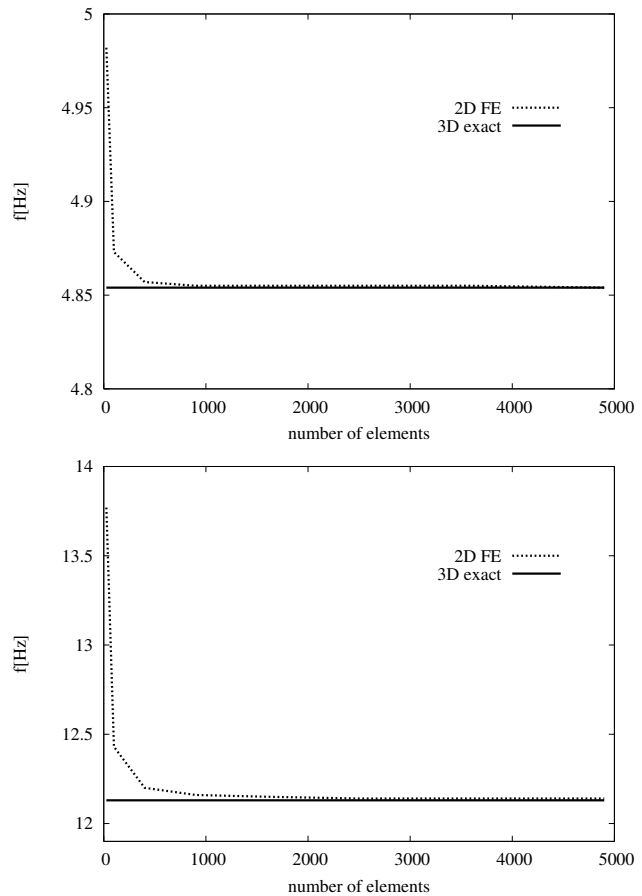


Figure 4: First assessment for the 2D FE solution, simply supported plate made of aluminium alloy with thickness ratio $a/h=1000$. Frequency f [Hz] vs. number of elements for the mode (1,1) (at the top) and for the mode (1,2) (at the bottom).

FE results with a rare mesh give bigger frequencies than 3D exact results. FE results converge to the 3D solution when the mesh increases. There is a very small error (always $\Delta(\%) \leq 0.18\%$) when the mesh is 127×38 . All these results are confirmed in graphical form in Figures 8 and 9.

The 2D FE model has been validated for both geometries (plates and cylinders) and for several lamination sequences (one-layered, two-layered and three-layered structures embedding isotropic or orthotropic materials). The FE model correctly converges with a 70×70 mesh for the plate geometry, and with a 127×38 mesh for the cylinder. Such values will always be used in Section 4 for the detailed comparison between the 3D exact solution and the 2D computational model.

Table 5: First assessment for the 2D FE solution, simply supported plate made of aluminium alloy with thickness ratios $a/h=1000$ and $a/h=100$. First two frequencies in Hz, comparison between the present 3D exact solution and the 2D FE solution via Nastran. The error is calculated as $\Delta(\%) = \frac{FE-3D}{3D} \times 100$.

a/h=1000							
		Mode I (1,1)			Mode I (1,2)		
Mesh	Num.El.	2D FE	3D	$\Delta(\%)$	2D FE	3D	$\Delta(\%)$
5×5	25	4.982	4.854	2.64	13.77	12.13	13.5
10×10	100	4.873	4.854	0.39	12.43	12.13	2.47
20×20	400	4.857	4.854	0.06	12.20	12.13	0.58
30×30	900	4.855	4.854	0.02	12.16	12.13	0.25
40×40	1600	4.855	4.854	0.02	12.15	12.13	0.16
50×50	2500	4.855	4.854	0.02	12.14	12.13	0.08
60×60	3600	4.855	4.854	0.02	12.14	12.13	0.08
70×70	4900	4.854	4.854	0.00	12.14	12.13	0.08
a/h=100							
		Mode I (1,1)			Mode I (1,2)		
Mesh	Num.El.	2D FE	3D	$\Delta(\%)$	2D FE	3D	$\Delta(\%)$
5×5	25	49.70	48.52	2.43	136.8	121.2	12.9
10×10	100	48.67	48.52	0.31	123.9	121.2	2.23
20×20	400	48.55	48.52	0.06	121.8	121.2	0.49
30×30	900	48.54	48.52	0.04	121.5	121.2	0.25
40×40	1600	48.53	48.52	0.02	121.4	121.2	0.16
50×50	2500	48.53	48.52	0.02	121.4	121.2	0.16
60×60	3600	48.53	48.52	0.02	121.3	121.2	0.08
70×70	4900	48.53	48.52	0.02	121.3	121.2	0.08

4 Results

This section proposes a detailed comparison between the 3D exact model discussed in this paper and 2D FE models obtained via the code MSC Nastran & Patran [8]. As demonstrated in the sections about the validation of the models, all the 3D exact results use an order of expansion $N=3$ for the exponential matrix, and $P=100$ fictitious layers for one-layered, two-layered and four-layered structures or $P=102$ fictitious layers for three-layered geometries. The 2D FE results use the SHELL QUAD4 element of Nastran with a 70×70 mesh for all the plate geometries and a 127×38 mesh for all the cylinder geometries. The comparisons will be made only for plates and cylinders in order to focus our attention to several laminations and materials. In this way, we are able to contain the length of the paper and we do not lose in clarity. For shell geometries, frequencies with $w \neq 0$ are obtained twice by Nastran (for each couple of (m,n)) because the section of the cylinder is symmetric. However, these two vibration modes are equal and we will write only one frequency in the table. Further geometries, such as cylindrical and spherical shell panels, that have already

been validated in Section 2.1 via the 3D exact model, could be the topic of a future comparison work.

4.1 Comparison between the two models

The first geometry considered in this investigation is a simply supported square plate with dimensions $a=b=1$ m. Thickness values are $h=0.1$ m, 0.05 m, 0.01 m and 0.001 m that mean thickness ratios $a/h=10$, 20 , 100 and 1000 , respectively. The second geometry is a simply supported cylinder with radii of curvature $R_\alpha=10$ m and $R_\beta=\infty$. The dimensions are $a=2\pi R_\alpha$ and $b=20$ m. The thickness values are $h=0.01$ m, 0.1 m, 1 m and 2 m that mean thickness ratios $R_\alpha/h=1000$, 100 , 10 and 5 , respectively. Both geometries will be considered as isotropic one-layered ($h_1 = h$), isotropic two-layered ($h_1 = h_2 = h/2$), isotropic three-layered ($h_1 = h_2 = h_3 = h/3$), three-layered composite cross-ply $90^\circ/0^\circ/90^\circ$ ($h_1 = h_2 = h_3 = h/3$), four-layered composite cross-ply $90^\circ/0^\circ/90^\circ/0^\circ$ ($h_1 = h_2 = h_3 = h_4 = h/4$) and three-layered sandwich (skins with $h_1 = h_3 = 0.2h$ and core with $h_2 = 0.6h$). The one-layered structures embed an aluminium alloy with Young modulus $E=73$ GPa, Poisson ratio $\nu=0.3$ and mass density

Table 6: Second assessment for the 2D FE solution, simply supported cylinder made of aluminium alloy and titanium alloy with thickness ratios $R_\alpha/h=1000$ and $R_\alpha/h=100$. First two frequencies in Hz, comparison between the present 3D exact solution and the 2D FE solution via Nastran. The error is calculated as $\Delta(\%) = \frac{FE-3D}{3D} \times 100$.

$R_\alpha/h=1000$							
		Mode I (18,1)			Mode I (20,1)		
Mesh	Num.El.	2D FE	3D	$\Delta(\%)$	2D FE	3D	$\Delta(\%)$
20×6	120	4.207	3.518	19.6	4.366	3.540	23.3
40×12	480	3.547	3.518	0.82	3.573	3.540	0.93
60×18	1080	3.523	3.518	0.14	3.542	3.540	0.06
70×21	1470	3.521	3.518	0.08	3.540	3.540	0.00
90×27	2430	3.519	3.518	0.03	3.538	3.540	-0.06
110×33	3630	3.518	3.518	0.00	3.538	3.540	-0.06
120×36	4320	3.518	3.518	0.00	3.538	3.540	-0.06
127×38	4826	3.518	3.518	0.00	3.538	3.540	-0.06
$R_\alpha/h=100$							
		Mode I (10,1)			Mode I (12,1)		
Mesh	Num.El.	2D FE	3D	$\Delta(\%)$	2D FE	3D	$\Delta(\%)$
20×6	120	11.01	10.76	2.32	12.15	11.65	4.11
40×12	480	10.76	10.76	0.00	11.61	11.65	-0.34
60×18	1080	10.75	10.76	-0.09	11.62	11.65	-0.26
70×21	1470	10.75	10.76	-0.09	11.62	11.65	-0.26
90×27	2430	10.75	10.76	-0.09	11.63	11.65	-0.17
110×33	3630	10.76	10.76	0.00	11.64	11.65	-0.08
120×36	4320	10.76	10.76	0.00	11.64	11.65	-0.08
127×38	4826	10.76	10.76	0.00	11.64	11.65	-0.08

$\rho = 2800 \text{ kg/m}^3$. The two-layered structures have the bottom layer in aluminum alloy and the top layer in titanium alloy ($E=114 \text{ GPa}$, $\nu = 0.3$ and $\rho = 2768 \text{ kg/m}^3$). The three-layered isotropic structures have the bottom layer in aluminum alloy, the mid layer in titanium alloy and the top layer in steel ($E=210 \text{ GPa}$, $\nu = 0.3$ and $\rho = 7850 \text{ kg/m}^3$). The composite material for the three-layered and four-layered cross-ply structures has Young moduli $E_1=132.38 \text{ GPa}$ and $E_2=E_3=10.756 \text{ GPa}$, shear moduli $G_{12}=G_{13}=5.6537 \text{ GPa}$ and $G_{23}=3.603 \text{ GPa}$, Poisson ratios $\nu_{12}=\nu_{13}=0.24$ and $\nu_{23}=0.49$, and mass density $\rho = 1600 \text{ kg/m}^3$. Sandwich configurations have the skins in aluminium alloy (see one-layered, two-layered and three-layered isotropic structures) and the core is in PVC ($E=0.18 \text{ GPa}$, $\nu=0.37$ and $\rho = 50 \text{ kg/m}^3$).

For all the benchmarks, the comparison is proposed calculating the first ten frequencies via the 2D FE code. From the visualization of these ten vibrations modes, it is possible to understand the half-wave numbers in the α and β directions. Therefore, these half-wave numbers have been used to calculate the same ten frequencies via the 3D exact model. There are some frequencies missed by the FE code, but they have not been investigated via the 3D exact model because this is not the main aim of the paper. The

main aim of the paper is to understand the differences between the 2D FE and the 3D exact model for the first ten frequencies given by the 2D FE code. It is also important to understand what are the features that influence these differences (geometry of the structures, materials, lamination sequences, thickness ratios, order of frequencies, vibration modes).

The first benchmark considers a one-layered isotropic plate (see Table 8 and Figure 10). For plate geometry the first ten frequencies for thin structures ($a/h=1000$ and $a/h=100$) are obtained with all the possible combinations of half-wave numbers in α and β directions from 1 to 4. The 3D model obtains such frequencies as the first mode for each couple of (m,n) . The FE code works very well for thin plates ($a/h=1000$ and 100), where the error is meaningless (always less than 0.3%) for all the first ten frequencies. In the case of thick plates ($a/h=20$ and 10), the FE code works well only for low frequencies and it gives significant errors for higher order frequencies (reaching an error of 2.31% for the tenth frequency of the $a/h=10$ plate). For thick plates, the FE code gives some modes that have the transverse displacement $w=0$ (they are in-plane modes). The 3D model also gives such values (mode II for

Table 7: Third assessment for the 2D FE solution, simply supported composite cylinder $90^\circ/0^\circ/90^\circ$ with thickness ratios $R_\alpha/h=1000$ and $R_\alpha/h=100$. First two frequencies in Hz, comparison between the present 3D exact solution and the 2D FE solution via Nastran. The error is calculated as $\Delta(\%) = \frac{FE-3D}{3D} \times 100$.

$R_\alpha/h=1000$							
		Mode I (22,1)			Mode I (24,1)		
Mesh	Num.El.	2D FE	3D	$\Delta(\%)$	2D FE	3D	$\Delta(\%)$
20×6	120	4.224	2.743	54.0	4.514	2.754	63.9
40×12	480	2.829	2.743	3.13	2.830	2.754	2.76
60×18	1080	2.771	2.743	1.02	2.774	2.754	0.73
70×21	1470	2.763	2.743	0.73	2.767	2.754	0.47
90×27	2430	2.754	2.743	0.40	2.760	2.754	0.22
110×33	3630	2.750	2.743	0.25	2.757	2.754	0.11
120×36	4320	2.749	2.743	0.22	2.756	2.754	0.07
127×38	4826	2.748	2.743	0.18	2.755	2.754	0.04
$R_\alpha/h=100$							
		Mode I (12,1)			Mode I (10,1)		
Mesh	Num.El.	2D FE	3D	$\Delta(\%)$	2D FE	3D	$\Delta(\%)$
20×6	120	8.271	7.717	7.18	8.653	8.151	6.16
40×12	480	7.783	7.717	0.85	8.250	8.151	1.21
60×18	1080	7.740	7.717	0.30	8.193	8.151	0.51
70×21	1470	7.734	7.717	0.22	8.182	8.151	0.38
90×27	2430	7.727	7.717	0.13	8.170	8.151	0.23
110×33	3630	7.724	7.717	0.09	8.163	8.151	0.15
120×36	4320	7.723	7.717	0.08	8.162	8.151	0.13
127×38	4826	7.722	7.717	0.06	8.161	8.151	0.12

(0,1), (1,0) and (1,1) even if it also gives other frequencies that have not been calculated by the 2D FE code. For in-plane modes ($w=0$), the error obtained with the FE code is almost zero because the 3D effects are not important in vibration modes with $w=0$. Left part of Figure 10 shows the first five vibration modes with transverse displacement $w \neq 0$ obtained via the FE code. These modes are important to understand the half-wave numbers (m,n) to use for the 3D exact investigation. The 3D exact model gives the vibration modes in terms of displacement components u , v and w in the thickness direction z (right side of Figure 10) because the behavior in α and β directions is already known (via the imposed half-wave numbers (m,n) obtained from the FE analysis).

The second benchmark is a one-layered isotropic cylinder embedding the same material already seen for the benchmark 1. Frequencies and vibration modes are shown in Table 9. Even if the employed material is the same, the behavior is completely different due to the coupling caused by the radius of curvature R_α . For each thickness ratio the lowest frequency is obtained for different couples of half-wave numbers (m,n) , these values decrease when the thickness of the shell increases. For such a struc-

ture the vibration behavior is not a priori predictable because there is not a regular sequence of (m,n) that gives the first ten frequencies for thin structures ($R_\alpha/h=1000$ and $R_\alpha/h=100$). In this case, it is fundamental to obtain the first ten frequencies via the FE code because the mode visualization of Nastran allows to understand what are the half-wave numbers (m,n) to use in the 3D exact model. The cylinder has a symmetric geometry, for this reason for each couple of (m,n) the frequencies with $w \neq 0$ are twice given. However, only one value is written in the tables. For thin cylinders ($R_\alpha/h=1000$ and 100) the 2D FE results are coincident with the 3D exact results (the error $\Delta(\%)$ is always negligible). For thick cylinders ($R_\alpha/h=10$ and $R_\alpha/h=5$), there are some FE frequencies that are quite different from the corresponding 3D frequencies (see for example the tenth frequency for $R_\alpha/h = 10$). These differences are not a priori predictable because the frequencies do not monotonously increase with the increasing of half-wave numbers (m,n) . For thick cylinders, the 2D FE code gives some modes with $w=0$ that are also given by the 3D model.

The third benchmark considers a two-layered isotropic plate, see Table 10. In the plate case there is not

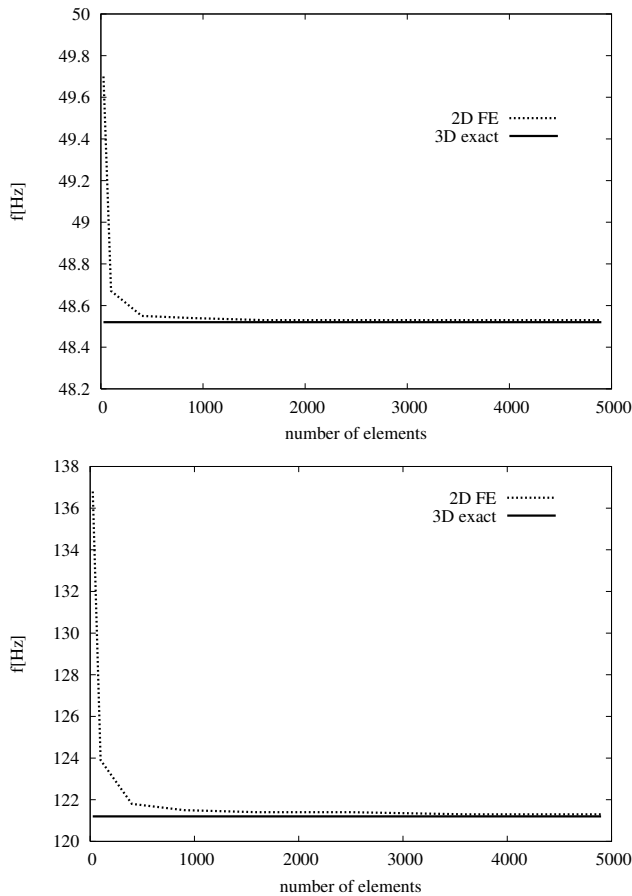


Figure 5: First assessment for the 2D FE solution, simply supported plate made of aluminium alloy with thickness ratio $a/h=100$. Frequency f [Hz] vs. number of elements for the mode (1,1) (at the top) and for the mode (1,2) (at the bottom).

any coupling due to the curvature, therefore the frequencies have the same behavior already seen for the benchmark 1 (they monotonously increase with the increasing of the half-wave numbers (m,n)). Therefore, the vibration behavior can be predicted for these structures. Errors for thin plates ($a/h=1000$ and 100) are small, but these errors for thick plates ($a/h=20$ and 10) are bigger even when low frequencies are investigated. For thick plates, there are some in-plane modes with $w=0$ that are coincident with the values given by the 3D model. However, some modes given by the 3D code have tragically been lost by the FE code (e.g., see mode I for $m=0$ and $n=1$ or $m=1$ and $n=0$ in the case of $a/h=20$ and $a/h=10$ plates).

The fourth benchmark analyzes the free vibrations for a simply supported two-layered isotropic cylinder. Results are shown in Table 11 and in Figure 11. The radius of curvature R_α gives a coupling between the displacement components. In this way, the vibration behavior is not a priori

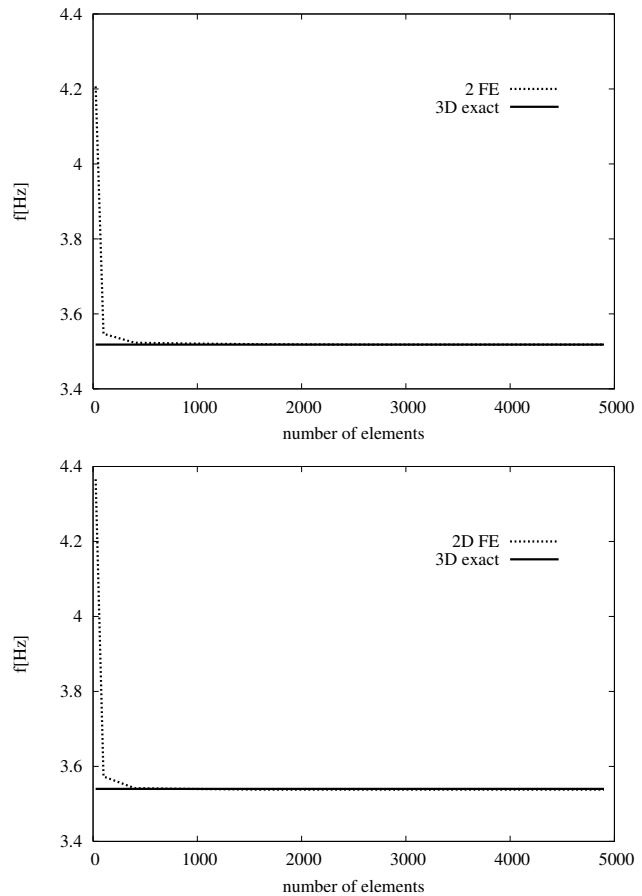


Figure 6: Second assessment for the 2D FE solution, simply supported multilayered cylinder made of aluminium alloy and titanium alloy with thickness ratio $R_\alpha/h=1000$. Frequency f [Hz] vs. number of elements for the mode (18,1) (at the top) and for the mode (20,1) (at the bottom).

predictable, as already seen for the second benchmark for the one-layered cylinder. The considerations are the same seen for the one-layered cylinder even if some errors given by the 2D FE model are bigger because there is a transverse anisotropy due the presence of these two different isotropic layers (see Table 11 for further details). Nastran gives some modes with $w=0$ for thick shells ($R_\alpha/h=10$ and $R_\alpha/h=5$). The 3D model gives such results but it also gives further frequencies that are not obtained by the 2D FE code (e.g., the mode I with $m=0$ and $n=1$ for $R_\alpha/h=5$). Figure 11 shows the first five frequencies with $w \neq 0$ obtained via Nastran (on the left side) and the corresponding first five frequencies with $w \neq 0$ obtained via the 3D exact model (on the right side). 3D modes are plotted only through the thickness direction because the behavior in α and β directions is known (imposed half-wave numbers (m,n)). However, all the first ten vibration modes given in the tables have been

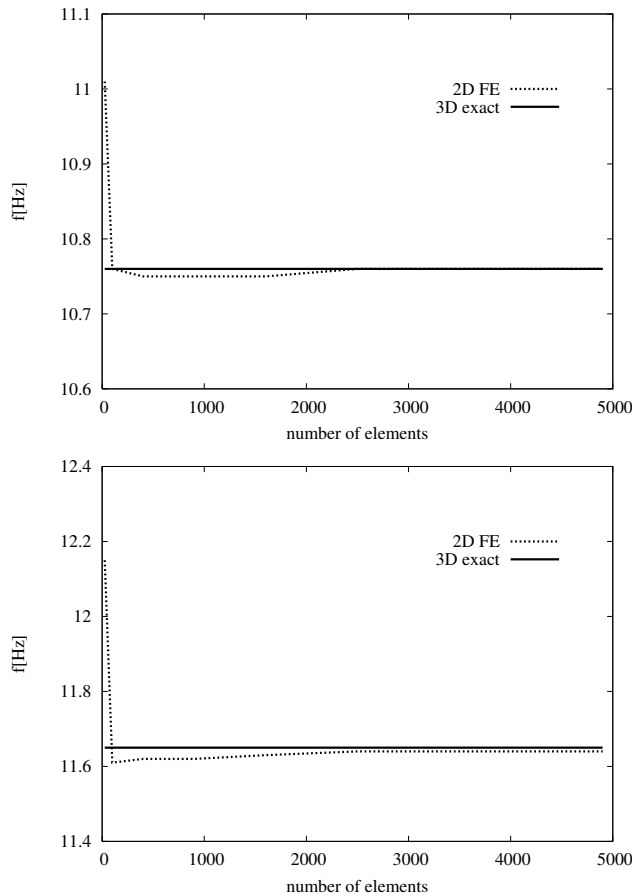


Figure 7: Second assessment for the 2D FE solution, simply supported multilayered cylinder made of aluminium alloy and titanium alloy with thickness ratio $R_\alpha/h=100$. Frequency f [Hz] vs. number of elements for the mode (10,1) (at the top) and for the mode (12,1) (at the bottom).

plotted via Nastran in order to make easier the comparison with the 3D exact results.

The fifth benchmark about a three-layered isotropic plate is discussed in Table 12 and in Figure 12. From the Table 12, it is clear how the behavior is similar to that already seen for the one-layered and two-layered plates even if the transverse anisotropy is different from the one-layered and two-layered cases. For the sake of clarity, the first five vibration modes with $w \neq 0$ are shown in Figure 12 for the 2D FE analysis (left side) and the 3D exact model (right side). The behavior is the same already seen for the first benchmark, the introduction of further layers does not change the vibration modes in terms of half-wave numbers (m,n) . For thick plates, the 2D FE code gives some in-plane modes ($w=0$) that are also calculated by the 3D model. However, the 3D model also gives further frequencies (e.g., for $m=1$

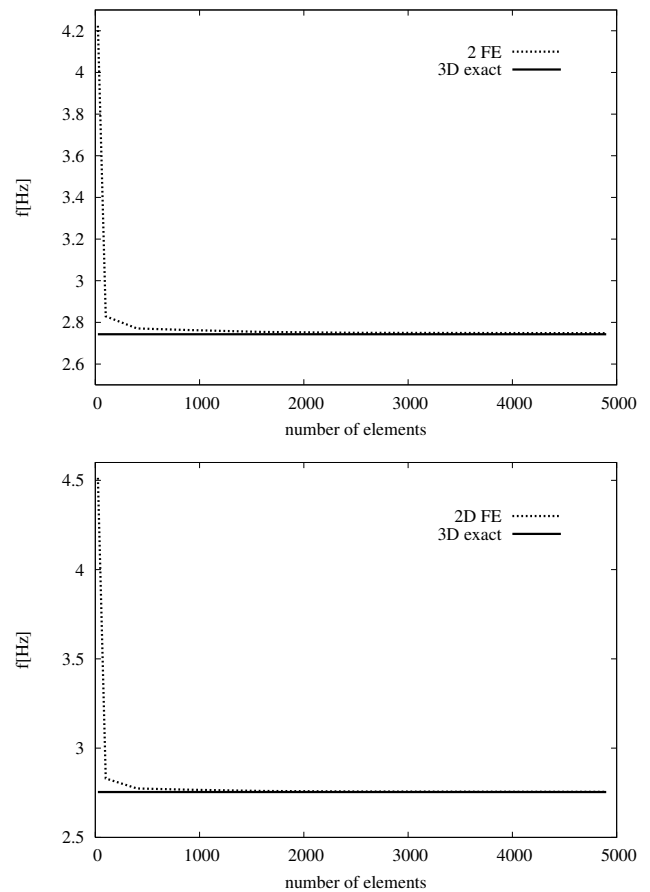


Figure 8: Third assessment for the 2D FE solution, simply supported composite cylinder $90^\circ/0^\circ/90^\circ$ with thickness ratio $R_\alpha/h=1000$. Frequency f [Hz] vs. number of elements for the mode (22,1) (at the top) and for the mode (24,1) (at the bottom).

and $n=0$, or $m=0$ and $n=1$) that have not been calculated by the 2D FE code.

The sixth benchmark proposes a three-layered isotropic cylinder (see Table 13), the behavior is the same already seen for the one-layered cylinder in benchmark two and for the two-layered cylinder in benchmark four. The behavior of the vibration modes obtained with the imposed half-wave numbers (m,n) is not a priori predictable. The presence of three different isotropic layers gives a bigger transverse anisotropy. Therefore, FE results give bigger errors, in particular for thicker structures and for some vibration modes. In the case of thick cylinder, there are some modes with transverse displacement $w=0$ that are not present for thin geometries.

The seventh benchmark considers a three-layered composite cross-ply $90^\circ/0^\circ/90^\circ$ plate. The frequency results for this symmetric laminated plate are given in Table 14. Even if a plate geometry is considered, the half-

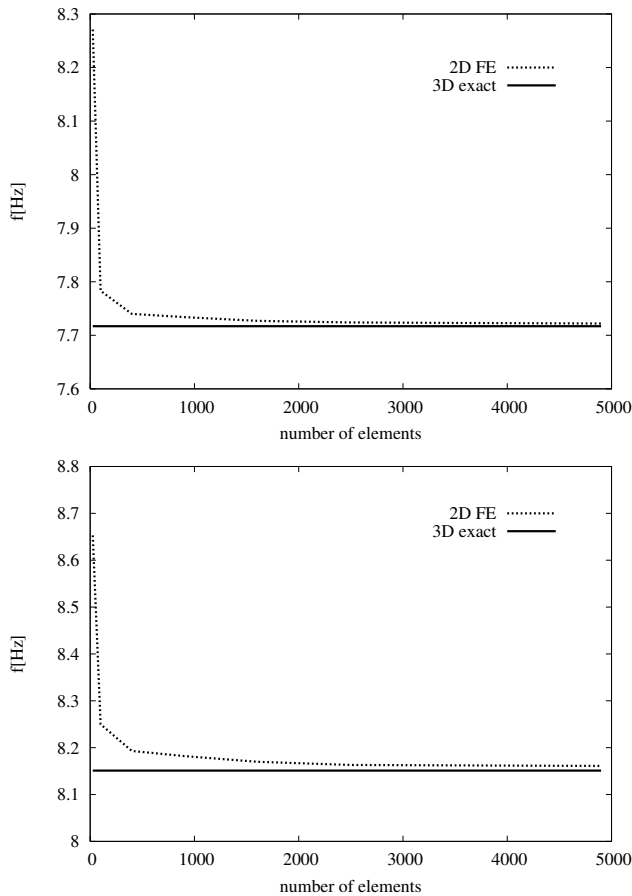


Figure 9: Third assessment for the 2D FE solution, simply supported composite cylinder $90^\circ/0^\circ/90^\circ$ with thickness ratio $R_\alpha/h=100$. Frequency f [Hz] vs. number of elements for the mode (12,1) (at the top) and for the mode (10,1) (at the bottom).

wave number (m,n) for the first ten frequencies are different with respect to the three-layered isotropic plate already proposed. This feature is due to the fact that there is an orthotropy. For this reason, the imposition of a certain value for half-wave number m in x direction is different from the n value in y direction. Therefore, the first ten frequencies for thin plates are not given by the first ten possible combinations of m and n from 1 to 4. For thick plates ($a/h=20$ and $a/h=10$), the FE code gives some in-plane modes with $w=0$. The 3D model also obtains such modes, but it also gives further vibration modes (e.g., the first ones for $(0,1)$ and $(0,2)$) that are not given by the FE code. The transverse anisotropy in the thickness direction is smaller than the isotropic cases that have three layers embedding different materials. For this reason, the errors given by the 2D FE model are smaller than errors seen in benchmarks three and five. Bigger errors are given for thick plate ($a/h=20$ and

10) but these errors are negligible for the in-plane modes with $w=0$ that have not any 3D effects.

The eight benchmark analyzes a three-layered composite cross-ply $90^\circ/0^\circ/90^\circ$ cylinder (see Table 15 and Figure 13). The errors given by the 2D FE code are smaller than those seen for benchmarks four and six. In fact, in the case of two-layered and three-layered isotropic cylinders the transverse anisotropy is bigger. The 2D FE code seems to give acceptable errors for all the thickness ratios and for each frequency (from the first to the tenth). The first five modes with transverse displacement $w \neq 0$ for this cylinder are shown in Figure 13 for both 2D FE and 3D exact analyses. There are not big differences with respect to the modes already plotted for the two-layered isotropic cylinder. The half-wave numbers (m,n) to calculate the first five modes with $w \neq 0$ change with respect to the isotropic case, but the general behavior remains the same. Some vibration modes with $w=0$ are calculated by the FE code in the case of thick cylinder. For thickness ratio $R_\alpha/h=5$, the FE code gives a mode with $w=0$ for $m=4$ and $n=0$. The 3D model also gives such a value but it also proposes a lower vibration mode for $m=4$ and $n=0$ that has not been calculated by the 3D FE code.

The four-layered composite cross-ply $90^\circ/0^\circ/90^\circ/0^\circ$ plate for the benchmark nine is analyzed in Table 16, and the first five vibration modes with transverse displacement $w \neq 0$ are given in Figure 14. In this case the lamination is not symmetric and the bottom 0° layer is able to compensate the behavior of the top 90° layer. For this reason, even if an orthotropic material is employed, results for half-wave numbers $(1,2)$ are equal to those for $(2,1)$, those for $(1,3)$ are equal to those for $(3,1)$, and so on. FE results are quite correct for each vibration mode. For thick plates ($a/h=20$ and $a/h=10$), the FE code gives some in-plane modes ($w=0$) for half-wave numbers $(0,1)$ and $(1,0)$, and $(0,2)$ and $(2,0)$. The 3D method also gives such frequencies but it also gives further modes (the first I for $(1,0)$, $(0,1)$, $(2,0)$ and $(0,2)$) that are not obtained by the FE code. Figure 14 about vibration modes with $w \neq 0$ confirm that the behavior is a priori predictable. The modes through the thickness show a transverse anisotropy (zigzag form of the displacements). However, this transverse anisotropy is small.

The tenth benchmark is about the four-layered composite cross-ply $90^\circ/0^\circ/90^\circ/0^\circ$ cylinder. Results shown in Table 17 confirm the same behavior already seen for the other cylinder configurations. Moreover, the errors obtained via the 2D FE analysis are smaller with respect to the two-layered and three-layered isotropic cases because there is a smaller transverse anisotropy. For the thick cases with $R_\alpha/h=10$ or 5, there are some vibration modes with $w=0$ for half-wave numbers $(2,0)$ and $(0,1)$. For $R_\alpha/h=5$

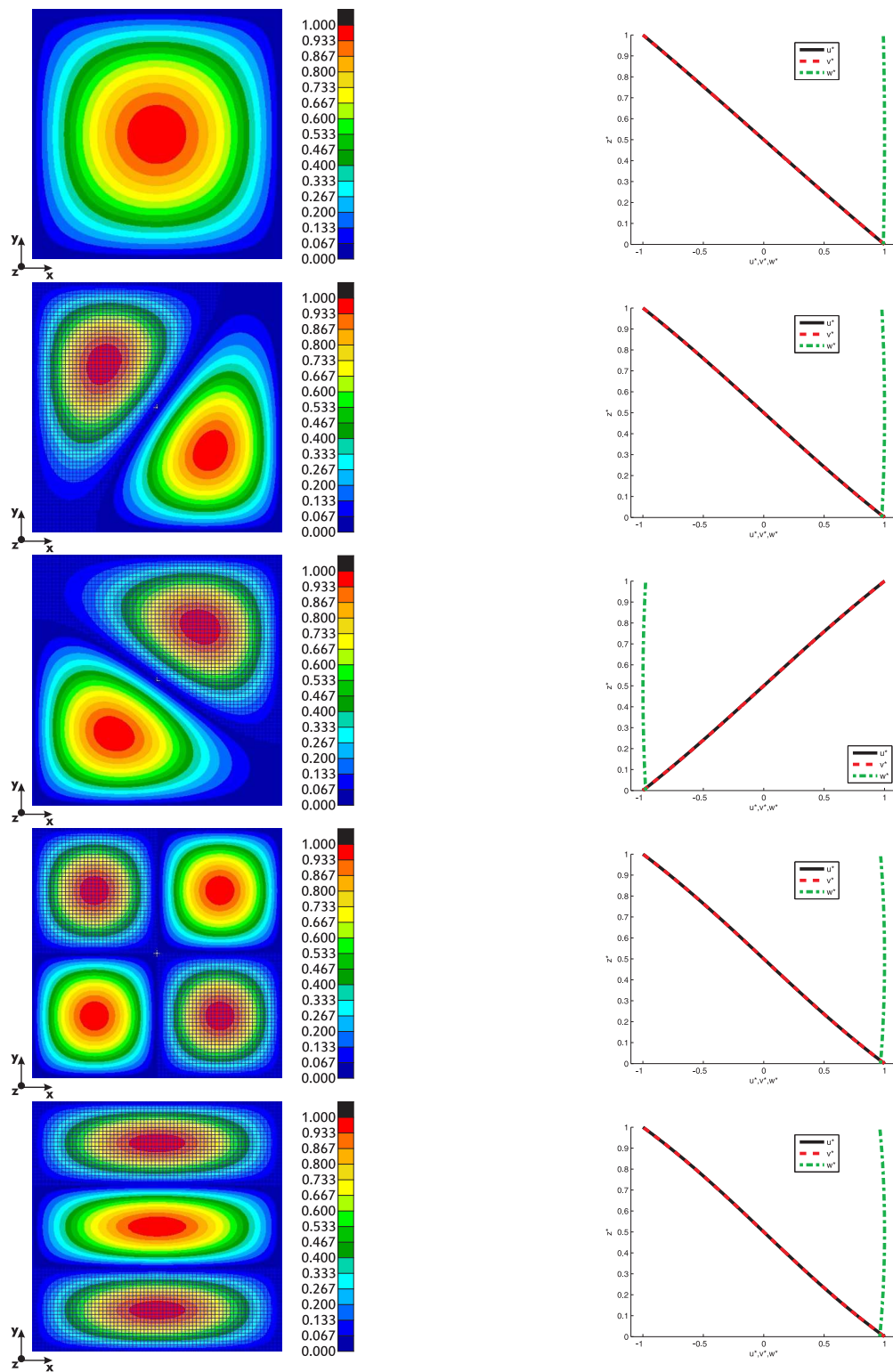


Figure 10: First benchmark, simply supported plate made of aluminium alloy with thickness ratio $a/h=10$. First five frequencies (with transverse displacement $w \neq 0$) via 2D FE solution (on the left) and via 3D exact solution (on the right).

shell, the FE code gives a frequency with $w=0$ for half-wave numbers (4,0). This frequency is also obtained by the 3D method. The 3D solution also gives another lower frequency for (4,0).

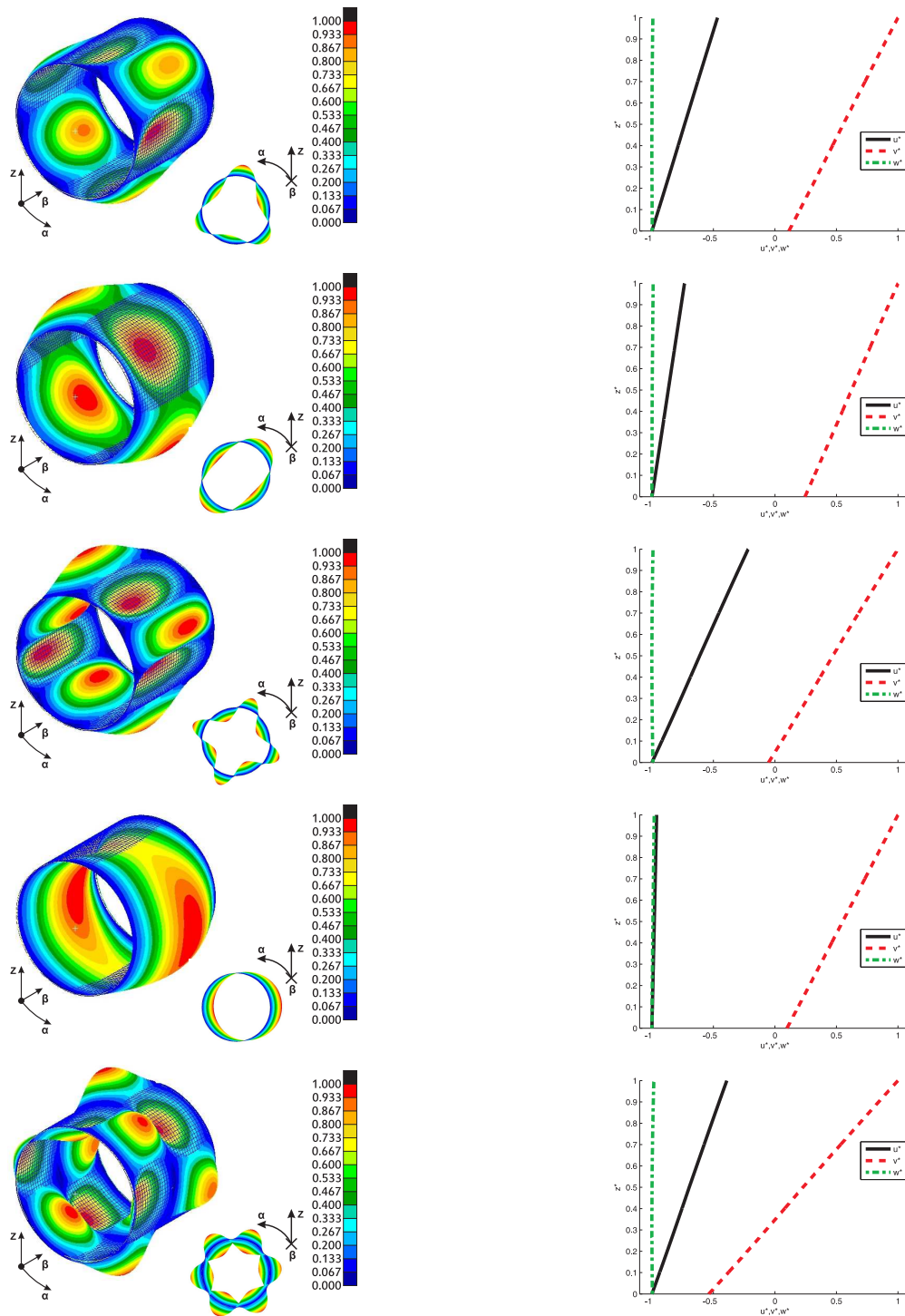


Figure 11: Fourth benchmark, simply supported cylinder made of aluminium alloy and titanium alloy with thickness ratio $R_\alpha/h=10$. First five frequencies (with transverse displacement $w \neq 0$) via 2D FE solution (on the left) and via 3D exact solution (on the right).

The eleventh benchmark considers a square sandwich plate with isotropic aluminium skins and an isotropic core in PVC. In this case the transverse anisotropy is very big because the elastic and mechanical properties of the core

are completely different from those of the skins. This feature is confirmed by the results given in Table 18. The errors given by the 2D FE code are acceptable only for thin plates ($a/h=1000$ or 100) but they are too large for thick

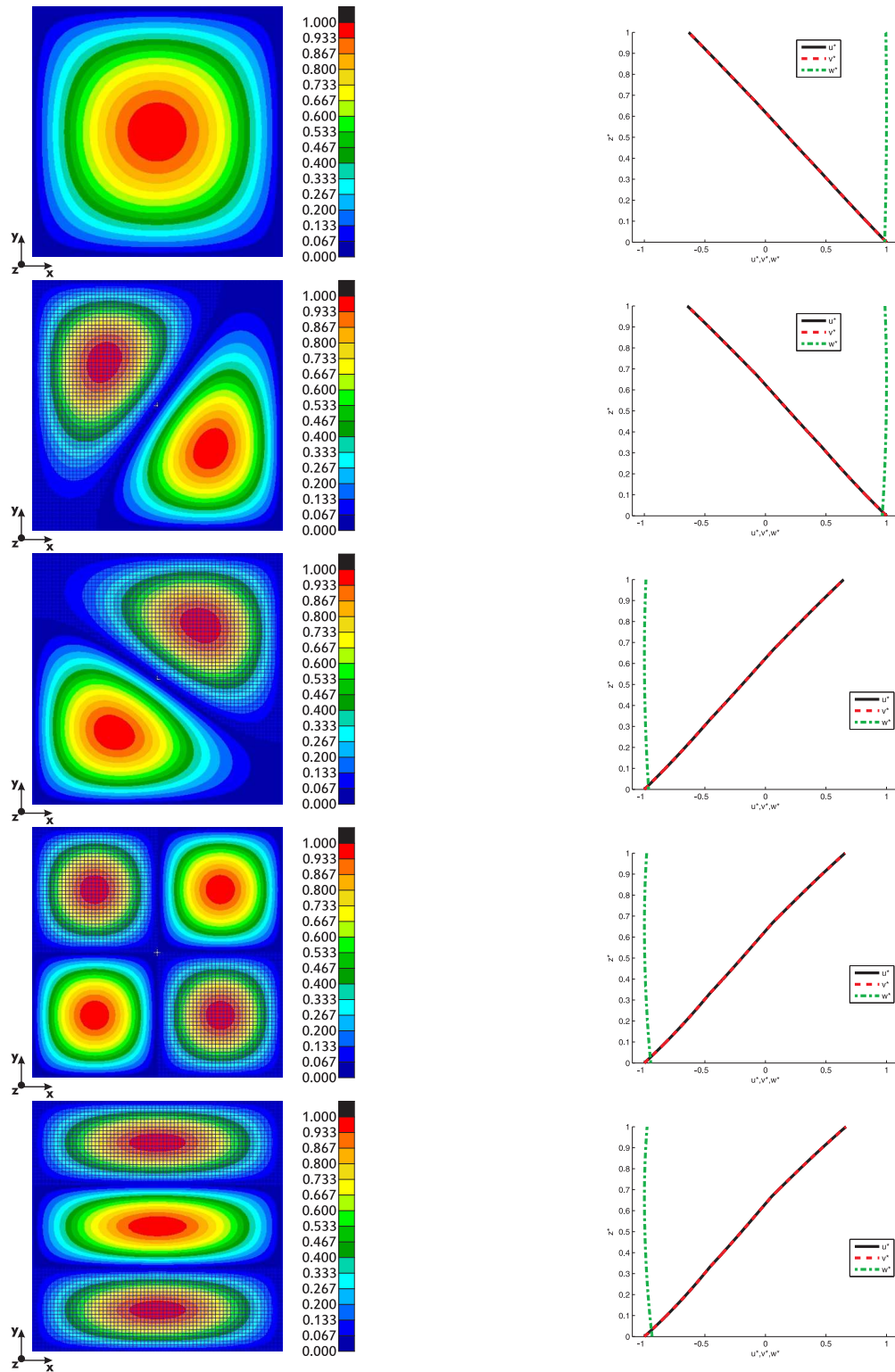


Figure 12: Fifth benchmark, simply supported plate made of aluminium alloy, titanium alloy and steel with thickness ratio $a/h=10$. First five frequencies (with transverse displacement $w \neq 0$) via 2D FE solution (on the left) and via 3D exact solution (on the right).

plates ($a/h=20$ or 10) for each frequency investigated (from the first to the tenth). The simple 2D kinematic model em-

ployed in the MSC Nastran code is not able to investigate thick and moderately thin sandwich structures with a big

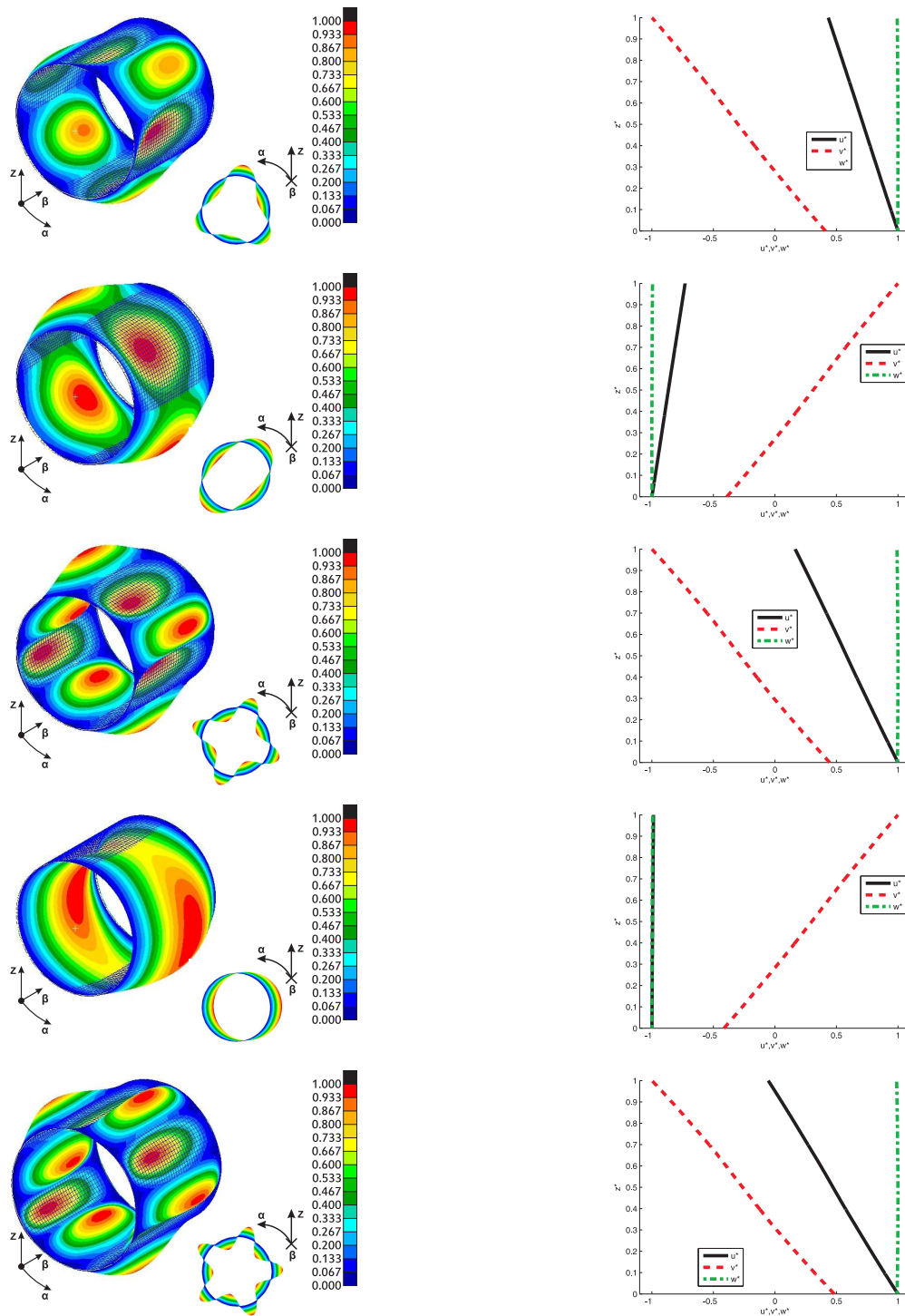


Figure 13: Eight benchmark, simply supported composite cylinder $90^\circ/0^\circ/90^\circ$ with thickness ratio $R_\alpha/h=10$. First five frequencies (with transverse displacement $w \neq 0$) via 2D FE solution (on the left) and via 3D exact solution (on the right).

transverse anisotropy. The 3D element of Nastran could give better results but is not used in this work because the main aim is the comparison between 3D exact models and 2D FE models. This 2D element of Nastran gives wrong

frequencies that are smaller than 3D results, and this feature demonstrates how the code does not work in a correct way for such a benchmark. The plate is isotropic in the plane and for this reason the vibration behavior is a priori

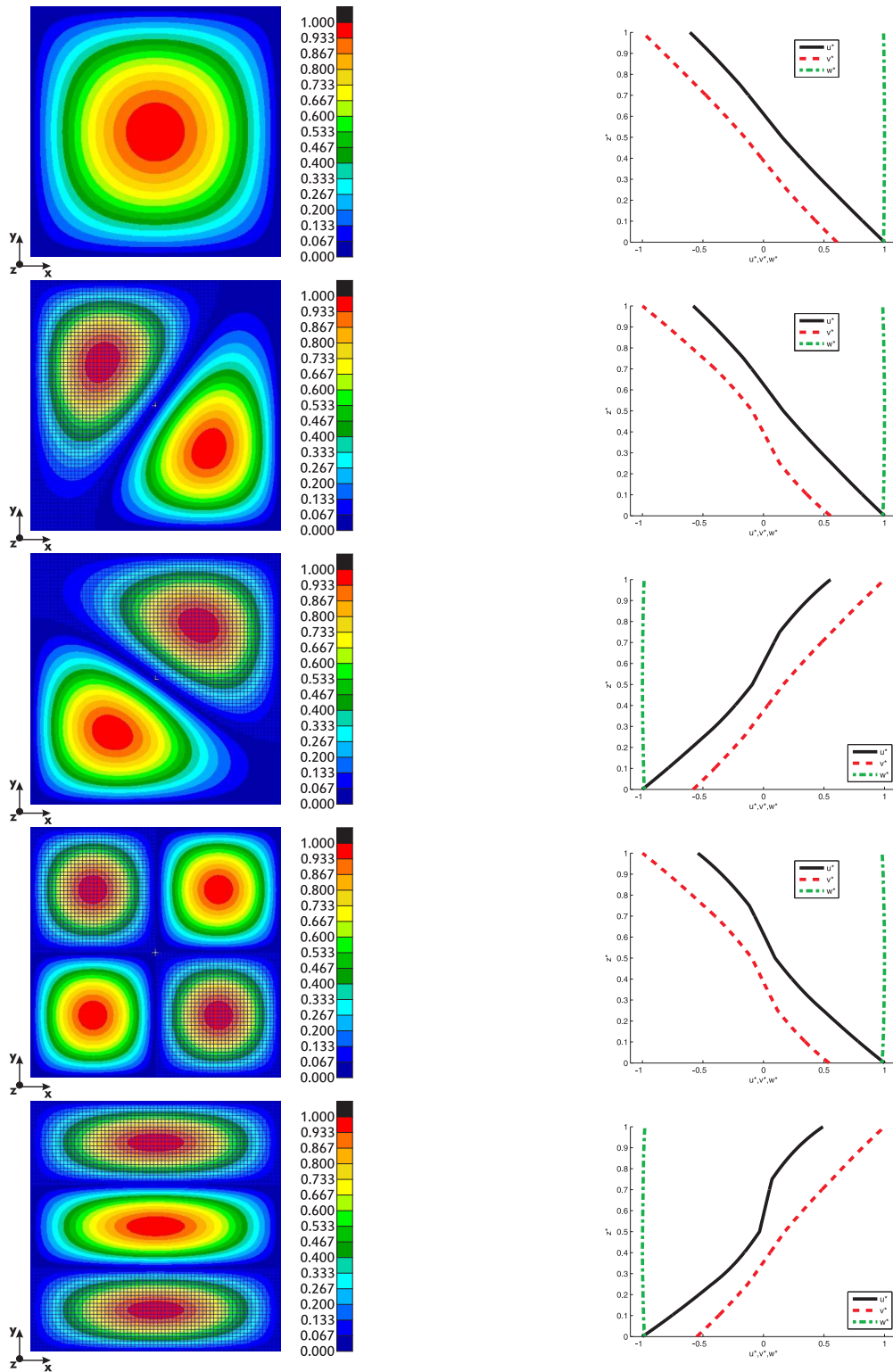


Figure 14: Ninth benchmark, simply supported composite plate $90^\circ/0^\circ/90^\circ/0^\circ$ with thickness ratio $a/h=10$. First five frequencies (with transverse displacement $w \neq 0$) via 2D FE solution (on the left) and via 3D exact solution (on the right).

predictable. In this benchmark, the FE code does not give any in-plane frequency (see all the thickness ratios a/h).

The same considerations seen in Table 18 for the sandwich plate are confirmed in Table 19 for the sand-

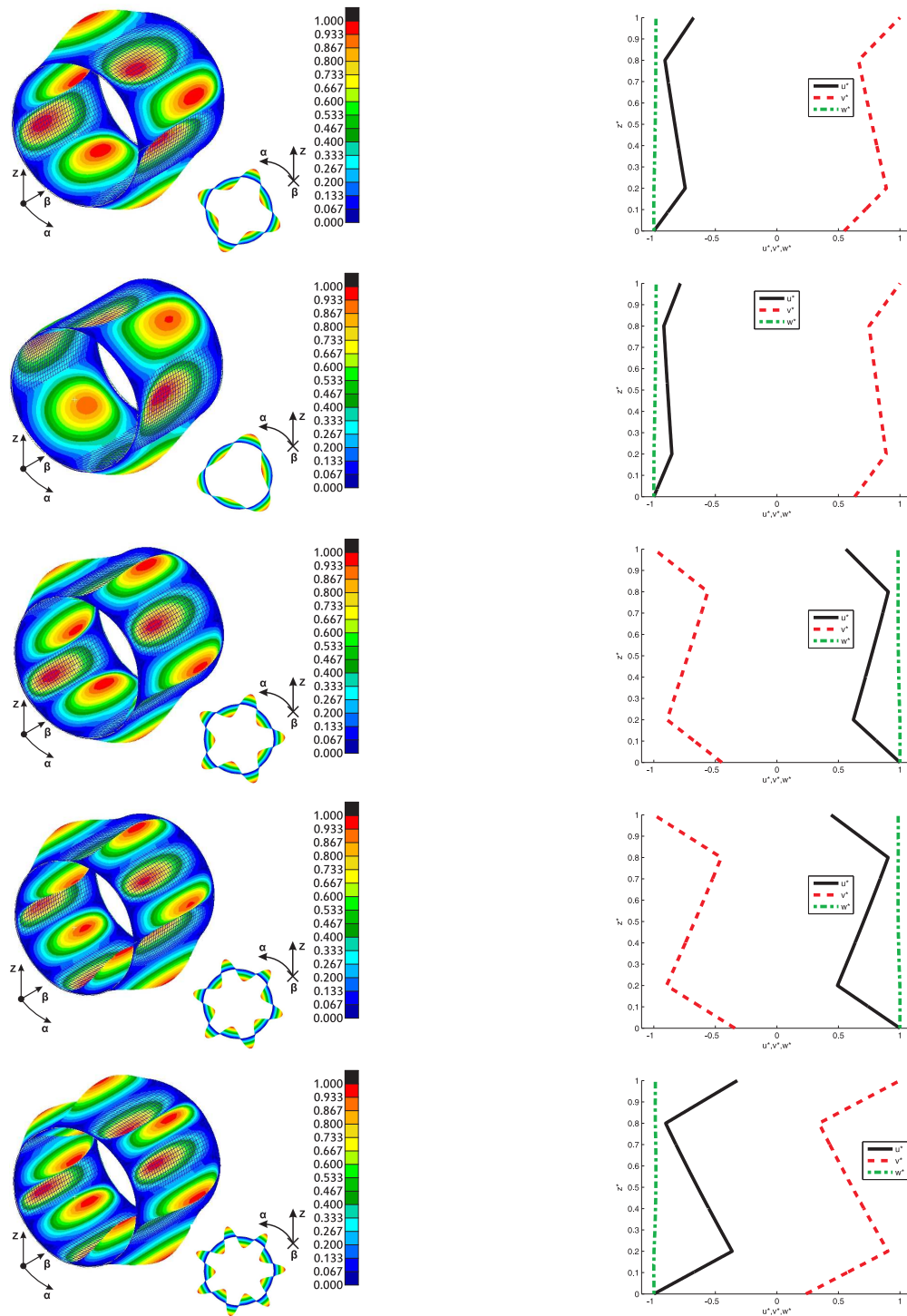


Figure 15: Twelfth benchmark, simply supported sandwich cylinder embedding isotropic skins and PVC core with thickness ratio $R_\alpha/h=10$. First five frequencies (with transverse displacement $w \neq 0$) via 2D FE solution (on the left) and via 3D exact solution (on the right).

wich cylinder. FE results are acceptable for thin shells ($R_\alpha/h=1000$ and 100) but they are completely wrong for thick shells ($R_\alpha/h=10$ and 5). This feature is due to the big transverse anisotropy of this configuration. This trans-

verse anisotropy is confirmed by Figure 15 where the first five frequencies with $w \neq 0$ obtained by the 3D exact model exhibit an important zigzag behavior for displacement components through the thickness. The cylinder is

isotropic but its behavior in terms of vibration modes and half-wave numbers is not easily predictable because of the coupling given by the radius of curvature R_α . In this last case there are not in-plane frequencies given by the FE code for thick cylinders. The FE results are completely wrong for thick shells as demonstrated by the values of frequency that are smaller than 3D values.

Figures 16-19 show how the first (I) 3D frequency values change with the half-wave numbers (m, n) in the case of simply supported one-layered and two-layered isotropic plates and cylinders. Figure 16 gives frequencies for one-layered isotropic plates with thickness ratios a/h equal 1000, 100 and 10. For $n=1$, frequency increases with the increasing of half-wave number m . The same behavior is confirmed for the curves related to $n=2$ and $n=3$. When n increases the curves move to higher values of frequency. Figure 17 shows frequencies for one-layered isotropic cylinders with thickness ratios R_α/h equal 1000, 100 and 10. The coupling between displacement components due to the curvature R_α gives the minimum value of frequency for a circumferential half-wave number different from one (e.g., $m=18$ for longitudinal half-wave number n equals 1 and thickness ratio $R_\alpha/h = 1000$). When the longitudinal half-wave number n increases, the curves move to higher values of frequency and the minimum in frequency moves to higher values of m . When the thickness ratio of the cylinder decreases (thicker shells), the values of circumferential half-wave number m that give the minimum of frequency also decrease. For example, for longitudinal half-wave number $n=1$, there is a minimum in frequency for $m=18$ for thickness ratio $R_\alpha/h = 1000$, $m=10$ for $R_\alpha/h = 100$, and $m=6$ for $R_\alpha/h = 10$. The behavior of the two-layered structures (Figures 18-19) is the same already seen for the corresponding one-layered structures (Figures 16-17), only the numerical values are different.

5 Conclusions

This paper has proposed an exact three-dimensional model for the free vibration analysis of one-layered and multilayered plates, cylinders, cylindrical and spherical shell panels. Comparisons with a commercial finite element code have been proposed (for the cases of plates and cylinders) in order to explain the method used for such a comparison and to see the possible differences between an exact 3D solution and a numerical 2D solution.

The exact 3D solution gives infinite vibration modes (for all the possible combinations of half-wave numbers (m, n)). A 2D FE code gives a finite number of vibration

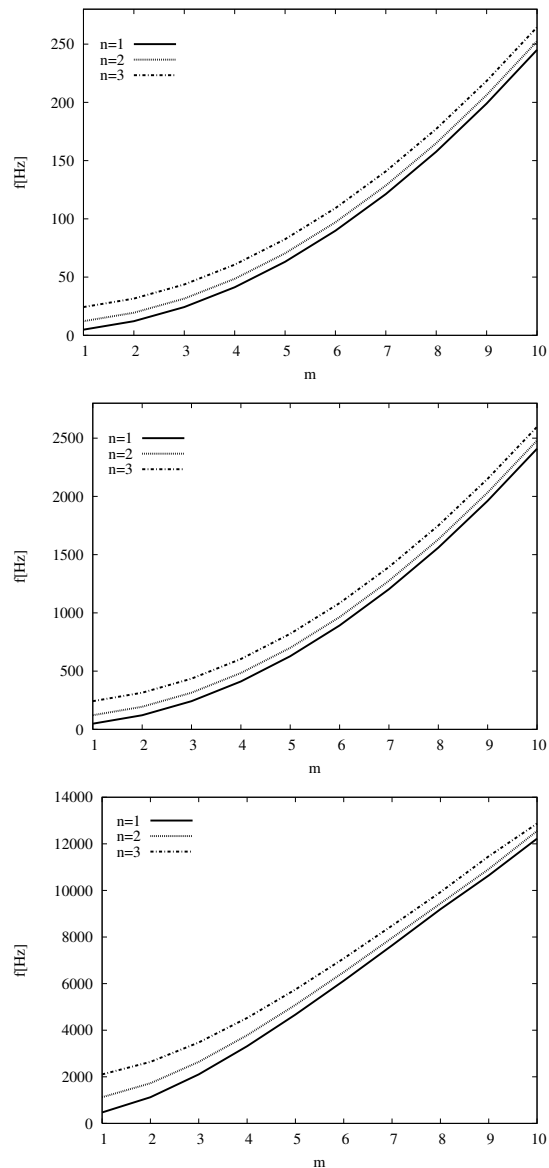


Figure 16: First benchmark, simply supported plate made of aluminium alloy with thickness ratios $a/h=1000$ (top), $a/h=100$ (middle) and $a/h=10$ (bottom). First (I) 3D frequencies versus half-wave numbers m (from 1 to 10) and n (from 1 to 3).

modes because it uses a finite number of degrees of freedom in the plane and in the thickness direction. A possible method to make a 3D versus 2D comparison is to calculate the frequencies via the 2D FE code and then to evaluate the 3D exact frequencies by means of the appropriate half-wave numbers (obtained via a correct visualization of the vibration modes via FE). It is obvious that the 3D analysis could give some frequencies that are missed by the 2D FE code, but this is not the aim of the paper. The paper tries to explain what could be the limitations of a commercial

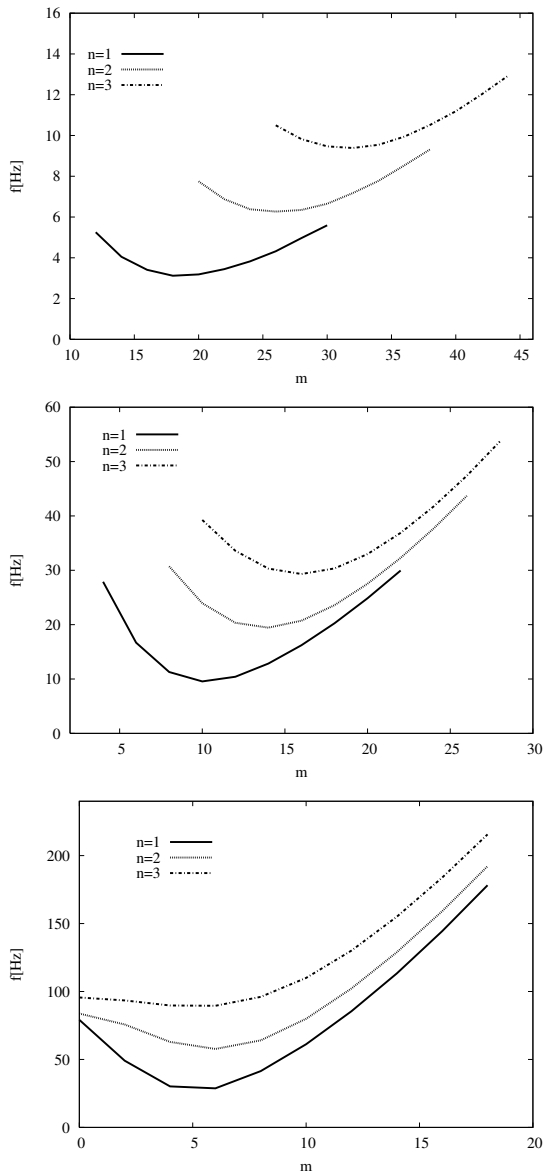


Figure 17: Second benchmark, simply supported cylinder made of aluminium alloy with thickness ratios $R_\alpha/h=1000$ (top), $R_\alpha/h=100$ (middle) and $R_\alpha/h=10$ (bottom). First (l) 3D frequencies versus half-wave numbers m (values around that for minimum frequency) and n (from 1 to 3).

2D FE code. A typical 2D FE code uses a Reissner-Mindlin model for the approximation of displacement components through the thickness direction. Results in this paper show how this model employed by commercial FE codes could give errors for thick and moderately thick structures, complicated lamination sequences, higher order frequencies and particular vibration modes. In these cases, the use of 3D finite elements or refined 2D finite elements is mandatory.

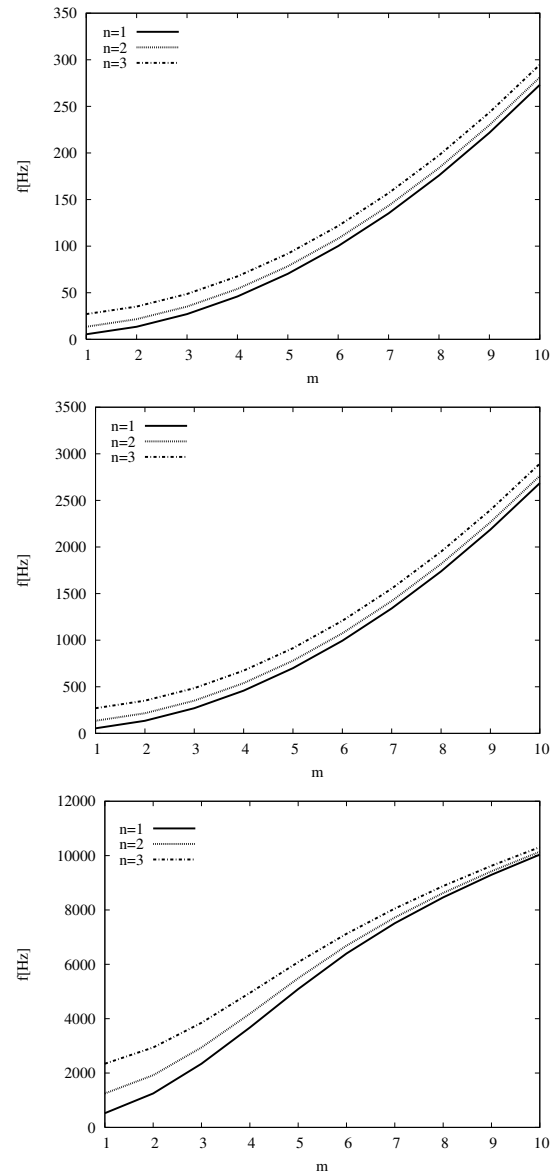


Figure 18: Third benchmark, simply supported plate embedding aluminium alloy and titanium alloy with thickness ratios $a/h=1000$ (top), $a/h=100$ (middle) and $a/h=10$ (bottom). First (l) 3D frequencies versus half-wave numbers m (from 1 to 10) and n (from 1 to 3).

The behavior of frequency values and vibration modes versus imposed half-wave numbers has been investigated via the 3D exact model. The behavior is simple and easily predictable for plate structures because the increasing of m and/or n values gives bigger frequency values. In the case of cylinder geometry there is a coupling between the displacement components due to the curvature. For this reason, when longitudinal half-wave number n is imposed, the minimum of frequency is obtained for a value of circumferential half-wave number m differ-

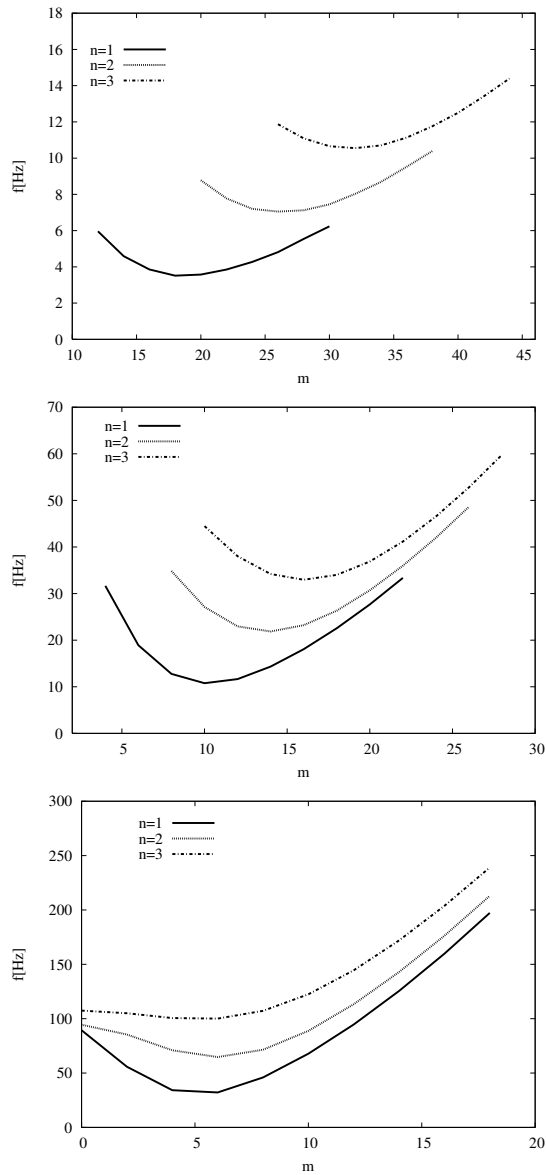


Figure 19: Fourth benchmark, simply supported cylinder embedding aluminium alloy and titanium alloy with thickness ratios $R_\alpha/h=1000$ (top), $R_\alpha/h=100$ (middle) and $R_\alpha/h=10$ (bottom). First (I) 3D frequencies versus half-wave numbers m (values around that for minimum frequency) and n (from 1 to 3).

ent from 1. Such values decrease when the thickness ratio decreases (thicker cylinders). When the longitudinal half-wave number n increases the curves frequency versus m move to higher values of frequencies and the minimum in frequency moves to higher values of the circumferential half-wave number m . These last considerations are very similar for one-layered and multilayered structures.

Table 8: First benchmark, simply supported plate made of aluminium alloy with thickness ratios $a/h=1000$, $a/h=100$, $a/h=20$ and $a/h=10$. First ten frequencies in Hz, comparison between the present 3D exact solution and the 2D FE solution via Nastran. The error is calculated as $\Delta(\%) = \frac{FE-3D}{3D} \times 100$.

2D FE	3D	Mode	m, n	$\Delta(\%)$
$a/h=1000$				
4.854	4.854	I	1,1	0.00
12.14	12.13	I	1,2	0.08
12.14	12.13	I	2,1	0.08
19.42	19.42	I	2,2	0.00
24.30	24.27	I	1,3	0.12
24.30	24.27	I	3,1	0.12
31.57	31.55	I	2,3	0.06
31.57	31.55	I	3,2	0.06
41.36	41.26	I	1,4	0.24
41.36	41.26	I	4,1	0.24
$a/h=100$				
48.53	48.52	I	1,1	0.02
121.3	121.2	I	1,2	0.08
121.3	121.2	I	2,1	0.08
194.0	193.9	I	2,2	0.05
242.7	242.3	I	1,3	0.16
242.7	242.3	I	3,1	0.16
315.1	314.8	I	2,3	0.09
315.1	314.8	I	3,2	0.09
412.6	411.4	I	1,4	0.29
412.6	411.4	I	4,1	0.29
$a/h=20$				
241.0	240.6	I	1,1	0.17
596.6	594.0	I	1,2	0.44
596.6	594.0	I	2,1	0.44
944.7	938.9	I	2,2	0.62
1174	1164	I	1,3	0.86
1174	1164	I	3,1	0.86
1511	1496	I	2,3	1.00
1511	1496	I	3,2	1.00
1584	1583	II($w=0$)	0,1	0.06
1584	1583	II($w=0$)	1,0	0.06
$a/h=10$				
472.3	469.5	I	1,1	0.60
1137	1122	I	1,2	1.34
1137	1122	I	2,1	1.34
1583	1583	II($w=0$)	0,1	0.00
1583	1583	II($w=0$)	1,0	0.00
1754	1724	I	2,2	1.74
2146	2102	I	1,3	2.09
2146	2102	I	3,1	2.09
2239	2239	II($w=0$)	1,1	0.00
2701	2640	I	2,3	2.31
2701	2640	I	3,2	2.31

Table 9: Second benchmark, simply supported cylinder made of aluminium alloy with thickness ratios $R_\alpha/h=1000$, $R_\alpha/h=100$, $R_\alpha/h=10$ and $R_\alpha/h=5$. First ten frequencies in Hz, comparison between the present 3D exact solution and the 2D FE solution via Nastran. The error is calculated as $\Delta(\%) = \frac{FE-3D}{3D} \times 100$.

2D FE	3D	Mode	m,n	$\Delta(\%)$
$R_\alpha/h=1000$				
3.123	3.123	I	18,1	0.00
3.153	3.154	I	20,1	-0.03
3.392	3.391	I	16,1	0.03
3.405	3.407	I	22,1	-0.06
3.813	3.816	I	24,1	-0.08
4.047	4.045	I	14,1	0.05
4.335	4.339	I	26,1	-0.09
4.942	4.947	I	28,1	-0.10
5.219	5.216	I	12,1	0.06
5.620	5.625	I	30,1	-0.09
$R_\alpha/h=100$				
9.557	9.558	I	10,1	-0.01
10.41	10.41	I	12,1	0.00
11.28	11.28	I	8,1	0.00
12.84	12.85	I	14,1	-0.08
16.20	16.22	I	16,1	-0.12
16.68	16.68	I	6,1	0.00
19.41	19.45	I	14,2	-0.21
20.23	20.26	I	18,1	-0.15
20.34	20.34	I	12,2	0.00
20.65	20.73	I	16,2	-0.39
$R_\alpha/h=10$				
28.74	28.72	I	6,1	0.07
30.21	30.19	I	4,1	0.07
41.45	41.42	I	8,1	0.07
49.07	49.08	I	2,1	-0.02
50.41	50.42	I(w=0)	2,0	-0.02
57.94	57.69	I	6,2	0.43
61.37	61.20	I	10,1	0.28
63.20	62.90	I	4,2	0.48
64.22	64.06	I	8,2	0.25
76.03	75.72	I	2,2	0.41
$R_\alpha/h=5$				
35.84	35.85	I	4,1	-0.03
47.58	47.66	I	6,1	-0.17
49.89	49.91	I	2,1	-0.04
50.42	50.48	I(w=0)	2,0	-0.12
75.03	74.93	I	8,1	0.13
79.40	78.47	I	4,2	1.18
79.41	79.16	I(w=0)	0,1	0.32
79.87	79.63	II	0,1	0.30
85.97	85.35	I	6,2	0.73
86.05	84.74	I	2,2	1.55

Table 10: Third benchmark, simply supported plate made of aluminium alloy and titanium alloy with thickness ratios $a/h=1000$, $a/h=100$, $a/h=20$ and $a/h=10$. First ten frequencies in Hz, comparison between the present 3D exact solution and the 2D FE solution via Nastran. The error is calculated as $\Delta(\%) = \frac{FE-3D}{3D} \times 100$.

2D FE	3D	Mode	m,n	$\Delta(\%)$
$a/h=1000$				
5.409	5.409	I	1,1	0.00
13.53	13.52	I	1,2	0.07
13.53	13.52	I	2,1	0.07
21.64	21.64	I	2,2	0.00
27.08	27.05	I	1,3	0.11
27.08	27.05	I	3,1	0.11
35.18	35.16	I	2,3	0.06
35.18	35.16	I	3,2	0.06
46.09	45.98	I	1,4	0.24
46.09	45.98	I	4,1	0.24
$a/h=100$				
54.08	54.07	I	1,1	0.02
135.2	135.1	I	1,2	0.07
135.2	135.1	I	2,1	0.07
216.2	216.1	I	2,2	0.05
270.4	270.0	I	1,3	0.15
270.4	270.0	I	3,1	0.15
351.2	350.8	I	2,3	0.11
351.2	350.8	I	3,2	0.11
459.8	458.4	I	1,4	0.30
459.8	458.4	I	4,1	0.30
$a/h=20$				
268.6	268.1	I	1,1	0.19
664.8	661.9	I	1,2	0.44
664.8	661.9	I	2,1	0.44
1053	1046	I	2,2	0.67
1309	1298	I	1,3	0.85
1309	1298	I	3,1	0.85
1684	1668	I	2,3	0.96
1684	1668	I	3,2	0.96
1797	1797	II(w=0)	0,1	0.00
1797	1797	II(w=0)	1,0	0.00
$a/h=10$				
526.3	523.1	I	1,1	0.61
1266	1250	I	1,2	1.28
1266	1250	I	2,1	1.28
1797	1797	II(w=0)	0,1	0.00
1797	1797	II(w=0)	1,0	0.00
1955	1922	I	2,2	1.72
2391	2344	I	1,3	2.00
2391	2344	I	3,1	2.00
2541	2540	II(w=0)	1,1	0.04
3010	2945	I	2,3	2.21
3010	2945	I	3,2	2.21

Table 11: Fourth benchmark, simply supported cylinder made of aluminium alloy and titanium alloy with thickness ratios $R_\alpha/h=1000$, $R_\alpha/h=100$, $R_\alpha/h = 10$ and $R_\alpha/h=5$. First ten frequencies in Hz, comparison between the present 3D exact solution and the 2D FE solution via Nastran. The error is calculated as $\Delta(\%) = \frac{FE-3D}{3D} \times 100$.

2D FE	3D	Mode	m,n	$\Delta(\%)$
$R_\alpha/h=1000$				
3.518	3.518	I	18,1	0.00
3.538	3.540	I	20,1	-0.06
3.810	3.812	I	22,1	-0.05
3.835	3.834	I	16,1	0.03
4.259	4.263	I	24,1	-0.09
4.585	4.583	I	14,1	0.04
4.837	4.841	I	26,1	-0.08
5.511	5.516	I	28,1	-0.09
5.920	5.917	I	12,1	0.05
6.265	6.271	I	30,1	-0.10
$R_\alpha/h=100$				
10.76	10.76	I	10,1	0.00
11.64	11.65	I	12,1	-0.09
12.78	12.77	I	8,1	0.08
14.31	14.33	I	14,1	-0.14
18.05	18.07	I	16,1	-0.11
18.93	18.92	I	6,1	0.05
21.81	21.86	I	14,2	-0.23
22.53	22.56	I	18,1	-0.13
22.96	22.97	I	12,2	-0.04
23.12	23.20	I	16,2	-0.34
$R_\alpha/h=10$				
32.07	32.11	I	6,1	-0.12
34.21	34.21	I	4,1	0.00
45.89	45.94	I	8,1	-0.11
55.81	55.77	I	2,1	0.07
57.05	57.07	I(w=0)	2,0	-0.03
65.01	64.74	I	6,2	0.42
67.80	67.78	I	10,1	0.03
71.37	70.94	I	4,2	0.61
71.52	71.41	I	8,2	0.15
86.03	85.43	I	2,2	0.70
$R_\alpha/h=5$				
40.33	40.39	I	4,1	-0.15
52.56	52.79	I	6,1	-0.44
56.83	56.76	I	2,1	0.12
56.91	56.99	I(w=0)	2,0	-0.14
82.46	82.61	I	8,1	-0.18
89.08	87.89	I	4,2	1.35
90.19	89.32	I	0,1	0.97
91.56	91.32	II(w=0)	0,1	0.26
95.68	95.04	I	6,2	0.67
96.93	95.00	I	2,2	2.03

Table 12: Fifth benchmark, simply supported plate made of aluminium alloy, titanium alloy and steel with thickness ratios $a/h=1000$, $a/h=100$, $a/h=20$ and $a/h=10$. First ten frequencies in Hz, comparison between the present 3D exact solution and the 2D FE solution via Nastran. The error is calculated as $\Delta(\%) = \frac{FE-3D}{3D} \times 100$.

2D FE	3D	Mode	m,n	$\Delta(\%)$
$a/h=1000$				
4.914	4.913	I	1,1	0.02
12.29	12.28	I	1,2	0.08
12.29	12.28	I	2,1	0.08
19.66	19.65	I	2,2	0.05
24.60	24.57	I	1,3	0.12
24.60	24.57	I	3,1	0.12
31.96	31.94	I	2,3	0.06
31.96	31.94	I	3,2	0.06
41.86	41.76	I	1,4	0.24
41.86	41.76	I	4,1	0.24
$a/h=100$				
49.12	49.12	I	1,1	0.00
122.8	122.7	I	1,2	0.08
122.8	122.7	I	2,1	0.08
196.3	196.3	I	2,2	0.00
245.6	245.2	I	1,3	0.16
245.6	245.2	I	3,1	0.16
318.9	318.6	I	2,3	0.09
318.9	318.6	I	3,2	0.09
417.6	416.4	I	1,4	0.29
417.6	416.4	I	4,1	0.29
$a/h=20$				
243.9	243.6	I	1,1	0.12
603.5	601.3	I	1,2	0.37
603.5	601.3	I	2,1	0.37
955.4	950.5	I	2,2	0.51
1187	1179	I	1,3	0.68
1187	1179	I	3,1	0.68
1527	1515	I	2,3	0.79
1527	1515	I	3,2	0.79
1687	1687	II(w=0)	0,1	0.00
1687	1687	II(w=0)	1,0	0.00
$a/h=10$				
477.6	475.2	I	1,1	0.50
1148	1136	I	1,2	1.06
1148	1136	I	2,1	1.06
1685	1687	II(w=0)	0,1	-0.12
1685	1687	II(w=0)	1,0	-0.12
1771	1745	I	2,2	1.49
2165	2129	I	1,3	1.69
2165	2129	I	3,1	1.69
2724	2673	I	2,3	1.91
2724	2673	I	3,2	1.91

Table 13: Sixth benchmark, simply supported cylinder made of aluminium alloy, titanium alloy and steel with thickness ratios $R_\alpha/h=1000$, $R_\alpha/h=100$, $R_\alpha/h = 10$ and $R_\alpha/h=5$. First ten frequencies in Hz, comparison between the present 3D exact solution and the 2D FE solution via Nastran. The error is calculated as $\Delta(\%) = \frac{FE-3D}{3D} \times 100$.

2D FE	3D	Mode	m,n	$\Delta(\%)$
$R_\alpha/h=1000$				
3.256	3.257	I	20,1	-0.03
3.259	3.259	I	18,1	0.00
3.487	3.489	I	22,1	-0.06
3.575	3.574	I	16,1	0.03
3.886	3.889	I	24,1	-0.08
4.292	4.290	I	14,1	0.05
4.404	4.408	I	26,1	-0.09
5.013	5.018	I	28,1	-0.10
5.551	5.548	I	12,1	0.05
5.695	5.701	I	30,1	-0.10
$R_\alpha/h=100$				
9.952	9.962	I	10,1	-0.10
10.65	10.67	I	12,1	-0.19
11.94	11.94	I	8,1	0.00
13.03	13.06	I	14,1	-0.23
16.40	16.43	I	16,1	-0.18
17.76	17.76	I	6,1	0.00
20.13	20.18	I	14,2	-0.25
20.45	20.50	I	18,1	-0.24
21.18	21.27	I	16,2	-0.42
21.36	21.38	I	12,2	-0.09
$R_\alpha/h=10$				
29.32	29.47	I	6,1	-0.51
31.98	31.99	I	4,1	-0.03
41.40	41.68	I	8,1	-0.67
52.49	52.17	I	2,1	0.61
53.38	53.07	I(w=0)	2,0	0.58
59.89	59.77	I	6,2	0.20
60.98	61.35	I	10,1	-0.60
65.08	65.26	I	8,2	-0.28
66.43	66.02	I	4,2	0.62
80.25	80.66	I	10,2	-0.51
$R_\alpha/h=5$				
37.33	37.41	I	4,1	-0.21
47.33	47.84	I	6,1	-1.07
53.08	52.50	I(w=0)	2,0	1.10
53.51	52.88	I	2,1	1.19
73.68	74.43	I	8,1	-1.01
81.95	80.89	I	4,2	1.31
84.12	83.04	I	0,1	1.30
86.93	86.66	I	6,2	0.31
87.36	84.05	I(w=0)	0,1	3.94
89.80	87.80	I	2,2	2.28

Table 14: Seventh benchmark, simply supported composite plate $90^\circ/0^\circ/90^\circ$ with thickness ratios $a/h=1000$, $a/h=100$, $a/h=20$ and $a/h=10$. First ten frequencies in Hz, comparison between the present 3D exact solution and the 2D FE solution via Nastran. The error is calculated as $\Delta(\%) = \frac{FE-3D}{3D} \times 100$.

2D FE	3D	Mode	m,n	$\Delta(\%)$
$a/h=1000$				
4.697	4.696	I	1,1	0.02
7.898	7.895	I	2,1	0.04
14.45	14.43	I	3,1	0.14
16.76	16.74	I	1,2	0.12
18.79	18.78	I	2,2	0.05
23.52	23.50	I	3,2	0.09
24.10	24.04	I	4,1	0.25
31.63	31.58	I	4,2	0.16
36.71	36.57	I	5,1	0.38
37.09	37.03	I	1,3	0.16
$a/h=100$				
46.90	46.89	I	1,1	0.02
78.87	78.83	I	2,1	0.05
144.2	143.9	I	3,1	0.21
166.6	166.5	I	1,2	0.06
186.9	186.8	I	2,2	0.05
234.0	233.7	I	3,2	0.13
240.2	239.5	I	4,1	0.29
314.6	313.9	I	4,2	0.22
365.4	363.7	I	5,1	0.47
366.1	365.5	I	1,3	0.16
$a/h=20$				
227.1	226.7	I	1,1	0.18
382.3	380.9	I	2,1	0.37
688.9	684.1	I	3,1	0.70
738.1	736.1	I	1,2	0.27
832.9	829.1	I	2,2	0.46
940.0	939.9	I(w=0)	0,1	0.01
1051	1043	I	3,2	0.77
1119	1107	I	4,1	1.08
1407	1393	I	4,2	1.00
1443	1440	I	1,3	0.21
$a/h=10$				
416.3	414.5	I	1,1	0.43
702.7	696.3	I	2,1	0.92
940.0	939.9	I(w=0)	0,1	0.01
1145	1144	I	1,2	0.09
1222	1205	I	3,1	1.41
1315	1308	I	2,2	0.53
1686	1668	I	3,2	1.08
1880	1880	I(w=0)	0,2	0.00
1882	1851	I	4,1	1.67
1959	1977	I	1,3	-0.91

Table 15: Eighth benchmark, simply supported composite cylinder $90^\circ/0^\circ/90^\circ$ with thickness ratios $R_\alpha/h=1000$, $R_\alpha/h=100$, $R_\alpha/h=10$ and $R_\alpha/h=5$. First ten frequencies in Hz, comparison between the present 3D exact solution and the 2D FE solution via Nastran. The error is calculated as $\Delta(\%) = \frac{FE-3D}{3D} \times 100$.

2D FE	3D	Mode	m,n	$\Delta(\%)$
$R_\alpha/h=1000$				
2.748	2.743	I	22,1	0.18
2.755	2.754	I	24,1	0.04
2.889	2.887	I	26,1	0.07
2.894	2.887	I	20,1	0.24
3.123	3.122	I	28,1	0.03
3.218	3.209	I	18,1	0.28
3.434	3.435	I	30,1	-0.03
3.748	3.738	I	16,1	0.27
3.807	3.809	I	32,1	-0.05
4.231	4.233	I	34,1	-0.05
$R_\alpha/h=100$				
7.722	7.717	I	12,1	0.06
8.161	8.151	I	10,1	0.12
8.407	8.406	I	14,1	0.01
9.919	9.923	I	16,1	-0.04
9.949	9.938	I	8,1	0.11
12.01	12.02	I	18,1	-0.08
13.44	13.43	I	6,1	0.07
14.53	14.54	I	20,1	-0.07
14.58	14.57	I	14,2	0.07
14.60	14.62	I	16,2	-0.14
$R_\alpha/h=10$				
20.79	20.81	I	6,1	-0.10
22.34	22.38	I	4,1	-0.18
26.29	26.27	I	8,1	0.08
29.92	29.93	I(w=0)	2,0	-0.03
32.61	32.64	I	2,1	-0.09
36.49	36.39	I	10,1	0.27
47.01	46.99	I(w=0)	0,1	0.04
47.27	47.28	I	6,2	-0.02
49.08	49.09	I	8,2	-0.02
49.73	49.51	I	12,1	0.44
$R_\alpha/h=5$				
27.54	27.65	I	4,1	-0.40
29.93	29.97	I(w=0)	2,0	-0.13
32.14	32.17	I	6,1	-0.09
34.47	34.56	I	2,1	-0.26
45.22	45.11	I	8,1	0.24
47.14	46.99	I(w=0)	0,1	0.32
59.84	59.93	II(w=0)	4,0	-0.15
63.20	62.90	I	10,1	0.48
65.21	65.39	I	4,2	-0.27
65.99	66.12	I	6,2	0.20

Table 16: Ninth benchmark, simply supported composite plate $90^\circ/0^\circ/90^\circ/0^\circ$ with thickness ratios $a/h=1000$, $a/h=100$, $a/h=20$ and $a/h=10$. First ten frequencies in Hz, comparison between the present 3D exact solution and the 2D FE solution via Nastran. The error is calculated as $\Delta(\%) = \frac{FE-3D}{3D} \times 100$.

2D FE	3D	Mode	m,n	$\Delta(\%)$
$a/h=1000$				
4.412	4.411	I	1,1	0.02
12.24	12.24	I	1,2	0.00
12.24	12.24	I	2,1	0.00
17.65	17.64	I	2,2	0.06
26.24	26.20	I	1,3	0.15
26.24	26.20	I	3,1	0.15
30.04	30.00	I	2,3	0.13
30.04	30.00	I	3,2	0.13
39.75	39.69	I	3,3	0.15
46.04	45.92	I	4,1	0.26
$a/h=100$				
44.07	44.06	I	1,1	0.02
122.0	121.9	I	1,2	0.08
122.0	121.9	I	2,1	0.08
175.8	175.7	I	2,2	0.06
260.4	259.9	I	1,3	0.19
260.4	259.9	I	3,1	0.19
298.1	297.7	I	2,3	0.13
298.1	297.7	I	3,2	0.13
393.8	393.3	I	3,3	0.13
454.3	452.9	I	4,1	0.31
$a/h=20$				
215.1	215.0	I	1,1	0.05
566.1	565.1	I	1,2	0.18
566.1	565.1	I	2,1	0.18
803.0	802.5	I	2,2	0.06
940.0	939.9	II(w=0)	0,1	0.01
940.0	939.9	II(w=0)	1,0	0.01
1116	1112	I	1,3	0.36
1116	1112	I	3,1	0.36
1277	1276	I	2,3	0.08
1277	1276	I	3,2	0.08
$a/h=10$				
401.3	401.3	I	1,1	0.00
940.0	939.9	II(w=0)	0,1	0.01
940.0	939.9	II(w=0)	1,0	0.01
947.2	947.9	I	1,2	-0.07
947.2	947.9	I	2,1	-0.07
1305	1312	I	2,2	-0.53
1655	1665	I	1,3	-0.60
1655	1665	I	3,1	-0.60
1880	1880	II(w=0)	0,2	0.00
1880	1880	II(w=0)	2,0	0.00

Table 17: Tenth benchmark, simply supported composite cylinder $90^\circ/0^\circ/90^\circ/0^\circ$ with thickness ratios $R_\alpha/h=1000$, $R_\alpha/h=100$, $R_\alpha/h = 10$ and $R_\alpha/h=5$. First ten frequencies in Hz, comparison between the present 3D exact solution and the 2D FE solution via Nastran. The error is calculated as $\Delta(\%) = \frac{FE-3D}{3D} \times 100$.

2D FE	3D	Mode	m,n	$\Delta(\%)$
$R_\alpha/h=1000$				
3.558	3.552	I	18,1	0.17
3.624	3.619	I	20,1	0.14
3.788	3.780	I	16,1	0.21
3.924	3.920	I	22,1	0.10
4.368	4.358	I	14,1	0.23
4.398	4.395	I	24,1	0.07
5.001	4.999	I	26,1	0.04
5.364	5.353	I	12,1	0.20
5.705	5.704	I	28,1	0.02
6.492	6.491	I	30,1	0.01
$R_\alpha/h=100$				
9.679	9.665	I	10,1	0.14
10.19	10.17	I	8,1	0.20
11.26	11.24	I	12,1	0.18
13.22	13.20	I	6,1	0.15
14.25	14.24	I	14,1	0.07
17.24	17.22	I	12,2	0.12
18.16	18.15	I	14,2	0.05
18.19	18.18	I	16,1	0.05
18.35	18.33	I	10,2	0.11
19.55	19.54	I	4,1	0.05
$R_\alpha/h=10$				
21.85	21.78	I	4,1	0.32
25.37	25.20	I	6,1	0.67
29.92	29.93	I(w=0)	2,0	-0.03
32.04	32.03	I	2,1	0.03
38.95	38.70	I	8,1	0.65
43.95	43.72	I	6,2	0.53
46.69	46.47	I	4,2	0.47
47.01	46.99	I(w=0)	0,1	0.04
51.63	51.44	I	8,2	0.37
57.21	56.89	I	10,1	0.56
$R_\alpha/h=5$				
26.73	26.54	I	4,1	0.72
29.93	29.97	I(w=0)	2,0	-0.13
32.81	32.78	I	2,1	0.09
38.93	38.63	I	6,1	0.78
47.14	46.99	I(w=0)	0,1	0.32
58.01	57.54	I	4,2	0.82
59.57	59.36	I	8,1	0.35
59.84	59.93	II(w=0)	4,0	-0.15
62.06	61.81	I	6,2	0.40
68.88	68.44	I	2,2	0.64

Table 18: Eleventh benchmark, simply supported sandwich plate embedding isotropic skins and PVC core with thickness ratios $a/h=1000$, $a/h=100$, $a/h=20$ and $a/h=10$. First ten frequencies in Hz, comparison between the present 3D exact solution and the 2D FE solution via Nastran. The error is calculated as $\Delta(\%) = \frac{FE-3D}{3D} \times 100$.

2D FE	3D	Mode	m,n	$\Delta(\%)$
$a/h=1000$				
6.705	6.704	I	1,1	0.01
16.75	16.74	I	1,2	0.06
16.75	16.74	I	2,1	0.06
26.77	26.76	I	2,2	0.04
33.47	33.43	I	1,3	0.12
33.47	33.43	I	3,1	0.12
43.43	43.41	I	2,3	0.05
43.43	43.41	I	3,2	0.05
56.82	56.69	I	1,4	0.23
56.82	56.69	I	4,1	0.23
$a/h=100$				
62.79	62.79	I	1,1	0.00
144.2	144.2	I	1,2	0.00
144.2	144.2	I	2,1	0.00
214.4	214.7	I	2,2	-0.14
256.8	257.3	I	1,3	-0.19
256.8	257.3	I	3,1	-0.19
314.7	315.9	I	2,3	-0.38
314.7	315.9	I	3,2	-0.38
384.6	386.4	I	1,4	-0.47
384.6	386.4	I	4,1	-0.47
$a/h=20$				
157.3	161.6	I	1,1	-2.66
267.0	287.6	I	1,2	-7.16
267.0	287.6	I	2,1	-7.16
344.4	387.5	I	2,2	-11.1
387.7	448.1	I	1,3	-13.5
387.7	448.1	I	3,1	-13.5
444.8	534.2	I	2,3	-16.7
444.8	534.2	I	3,2	-16.7
511.5	643.2	I	1,4	-20.5
511.5	643.2	I	4,1	-20.5
$a/h=10$				
172.1	193.7	I	1,1	-11.1
277.8	361.1	I	1,2	-23.1
277.8	361.1	I	2,1	-23.1
353.2	513.2	I	2,2	-31.2
395.7	611.6	I	1,3	-35.3
395.7	611.6	I	3,1	-35.3
451.9	756.7	I	2,3	-40.3
451.9	756.7	I	3,2	-40.3
517.7	947.5	I	1,4	-45.4
517.7	947.5	I	4,1	-45.4

Table 19: Twelfth benchmark, simply supported sandwich cylinder embedding isotropic skins and PVC core with thickness ratios $R_\alpha/h=1000$, $R_\alpha/h=100$, $R_\alpha/h = 10$ and $R_\alpha/h=5$. First ten frequencies in Hz, comparison between the present 3D exact solution and the 2D FE solution via Nastran. The error is calculated as $\Delta(\%) = \frac{FE-3D}{3D} \times 100$.

2D FE	3D	Mode	m,n	$\Delta(\%)$
$R_\alpha/h=1000$				
3.642	3.644	1	18,1	-0.05
3.687	3.687	1	16,1	0.00
3.919	3.922	1	20,1	-0.08
4.171	4.170	1	14,1	0.02
4.420	4.425	1	22,1	-0.11
5.075	5.082	1	24,1	-0.14
5.233	5.230	1	12,1	0.06
5.846	5.855	1	26,1	-0.15
6.709	6.721	1	28,1	-0.18
7.122	7.119	1	10,1	0.04
$R_\alpha/h=100$				
10.68	10.69	1	10,1	-0.09
11.68	11.68	1	8,1	0.00
12.18	12.19	1	12,1	-0.08
14.94	14.98	1	14,1	-0.27
16.63	16.62	1	6,1	0.06
18.32	18.40	1	16,1	-0.43
20.96	21.03	1	14,2	-0.33
21.40	21.41	1	12,2	-0.05
22.04	22.17	1	18,1	-0.59
22.37	22.51	1	16,2	-0.62
$R_\alpha/h=10$				
18.30	19.79	1	8,1	-7.53
19.63	20.04	1	6,1	-2.05
20.47	23.70	1	10,1	-13.6
23.85	29.48	1	12,1	-19.1
27.60	36.36	1	14,1	-24.1
28.41	28.46	1	4,1	-0.18
30.71	37.10	1	12,2	-17.2
31.26	34.84	1	10,2	-10.3
31.48	44.15	1	16,1	-28.7
32.15	42.10	1	14,2	-23.6
$R_\alpha/h=5$				
18.65	24.68	1	8,1	-24.4
19.91	21.93	1	6,1	-9.21
20.81	32.50	1	10,1	-36.0
24.15	42.96	1	12,1	-41.4
27.87	55.27	1	14,1	-49.6
28.57	28.83	1	4,1	-0.90
30.96	52.38	1	12,2	-40.9
31.50	44.69	1	10,2	-29.5
31.72	69.01	1	16,1	-54.0
32.39	63.30	1	14,2	-48.8

References

- [1] A.W. Leissa, *Vibration of Plates*, NASA SP-160, Washington, 1969.
- [2] A.W. Leissa, *Vibration of Shells*, NASA SP-288, Washington, 1973.
- [3] S. Werner, *Vibrations of Shells and Plates*, 3rd edition: revised and expanded, CRC Press, New York: Marcel Dekker Inc., 2004.
- [4] S. Brischetto and E. Carrera, Importance of higher order modes and refined theories in free vibration analysis of composite plates, *Journal of Applied Mechanics*, 77, 1-14, 2010.
- [5] S. Brischetto, Exact elasticity solution for natural frequencies of functionally graded simply-supported structures, *CMES: Computer Modeling in Engineering & Sciences*, 95, 391-430, 2013.
- [6] S. Brischetto, A continuum elastic three-dimensional model for natural frequencies of single-walled carbon nanotubes, *Composites Part B: Engineering*, 61, 222-228, 2014.
- [7] S. Brischetto, Three-dimensional exact free vibration analysis of spherical, cylindrical, and flat one-layered panels, *Shock and Vibration*, 2014, 1-29, 2014.
- [8] MSC Nastran, Products (<http://www.mscsoftware.com/product/msc-nastran>, accessed on 4th November 2014).
- [9] S. Aimmanee and R.C. Batra, Analytical solution for vibration of an incompressible isotropic linear elastic rectangular plate, and frequencies missed in previous solutions, *Journal of Sound and Vibration*, 302, 613-620, 2007.
- [10] R.C. Batra and S. Aimmanee, Letter to the Editor: Missing frequencies in previous exact solutions of free vibrations of simply supported rectangular plates, *Journal of Sound and Vibration*, 265, 887-896, 2003.
- [11] S. Srinivas, C.V. Joga Rao and A.K. Rao, An exact analysis for vibration of simply-supported homogeneous and laminated thick rectangular plates, *Journal of Sound and Vibration*, 12, 187-199, 1970.
- [12] S. Srinivas, A.K. Rao and C.V. Rao, Flexure of simply supported thick homogeneous and laminated rectangular plates, *Zeitschrift für Angewandte Mathematik und Mechanik*, 49, 449-458, 1969.
- [13] R.C. Batra, S. Vidoli and F. Vestroni, Plane wave solutions and modal analysis in higher order shear and normal deformable plate theories, *Journal of Sound and Vibration*, 257, 63-88, 2002.
- [14] J.Q. Ye, A three-dimensional free vibration analysis of cross-ply laminated rectangular plates with clamped edges, *Computer Methods in Applied Mechanics and Engineering*, 140, 383-392, 1997.
- [15] A. Messina, Three dimensional free vibration analysis of cross-ply laminated plates through 2D and exact models, *3rd International Conference on Integrity, Reliability and Failure*, Porto (Portugal), 20-24 July 2009.
- [16] Y.K. Cheung and D. Zhou, Three-dimensional vibration analysis of cantilevered and completely free isosceles triangular plates, *International Journal of Solids and Structures*, 39, 673-687, 2002.
- [17] K.M. Liew and B. Yang, Three-dimensional elasticity solutions for free vibrations of circular plates: a polynomials-Ritz analysis, *Computer Methods in Applied Mechanics and Engineering*, 175, 189-201, 1999.
- [18] Y.B. Zhao, G.W. Wei and Y. Xiang, Discrete singular convolution for the prediction of high frequency vibration of plates, *International Journal of Solids and Structures*, 39, 65-88, 2002.
- [19] G.W. Wei, Y.B. Zhao and Y. Xiang, A novel approach for the analysis of high-frequency vibrations, *Journal of Sound and Vibration*, 257, 207-246, 2002.
- [20] H. Rokni Damavandi Taher, M. Omid, A.A. Zadpoor and A.A. Nikooyan, Short Communication: Free vibration of circular and annular plates with variable thickness and different combinations of boundary conditions, *Journal of Sound and Vibration*, 296, 1084-1092, 2006.
- [21] Y. Xing and B. Liu, New exact solutions for free vibrations of rectangular thin plates by symplectic dual method, *Acta Mechanica Sinica*, 25, 265-270, 2009.
- [22] S.S. Vel and R.C. Batra, Three-dimensional exact solution for the vibration of functionally graded rectangular plates, *Journal of Sound and Vibration*, 272, 703-730, 2004.
- [23] W.-Q. Chen, H.-J. Ding and R.-Q. Xu, On exact analysis of free vibrations of embedded transversely isotropic cylindrical shells, *International Journal of Pressure Vessels and Piping*, 75, 961-966, 1998.
- [24] B. Gasemzadeh, R. Azarafza, Y. Sahebi and A. Motallebi, Analysis of free vibration of cylindrical shells on the basis of three dimensional exact elasticity theory, *Indian Journal of Science and Technology*, 5, 3260-3262, 2012.
- [25] N.N. Huang, Exact analysis for three-dimensional free vibrations of cross-ply cylindrical and doubly-curved laminates, *Acta Mechanica*, 108, 23-34, 1995.
- [26] J.N. Sharma, D.K. Sharma and S.S. Dhaliwal, Three-dimensional free vibration analysis of a viscothermoelastic hollow sphere, *Open Journal of Acoustics*, 2, 12-24, 2012.
- [27] J.N. Sharma and N. Sharma, Three-dimensional free vibration analysis of a homogeneous transversely isotropic thermoelastic sphere, *Journal of Applied Mechanics*, 77, 1-9, 2010.
- [28] K.P. Soldatos and J. Ye, Axisymmetric static and dynamic analysis of laminated hollow cylinders composed of monoclinic elastic layers, *Journal of Sound and Vibration*, 184, 245-259, 1995.
- [29] A.E. Armenakas, D.C. Gazis and G. Herrmann, *Free Vibrations of Circular Cylindrical Shells*, Pergamon Press, Oxford, 1969.
- [30] A. Bhimaraddi, A higher order theory for free vibration analysis of circular cylindrical shells, *International Journal of Solids and Structures*, 20, 623-630, 1984.
- [31] H. Zhou, W. Li, B. Lv and W.L. Li, Free vibrations of cylindrical shells with elastic-support boundary conditions, *Applied Acoustics*, 73, 751-756, 2012.
- [32] S.M.R. Khalili, A. Davar and K.M. Fard, Free vibration analysis of homogeneous isotropic circular cylindrical shells based on a new three-dimensional refined higher-order theory, *International Journal of Mechanical Sciences*, 56, 1-25, 2012.
- [33] S.S. Vel, Exact elasticity solution for the vibration of functionally graded anisotropic cylindrical shells, *Composite Structures*, 92, 2712-2727, 2010.
- [34] C.T. Loy and K.Y. Lam, Vibration of thick cylindrical shells on the basis of three-dimensional theory of elasticity, *Journal of Sound and Vibration*, 226, 719-737, 1999.
- [35] Y. Wang, R. Xu, H. Ding and J. Chen, Three-dimensional exact solutions for free vibrations of simply supported magneto-electro-elastic cylindrical panels, *International Journal of Engineering Science*, 48, 1778-1796, 2010.

- [36] E. Efraim and M. Eisenberger, Exact vibration frequencies of segmented axisymmetric shells, *Thin-Walled Structures*, 44, 281-289, 2006.
- [37] J.-H. Kanga and A.W. Leissa, Three-dimensional vibrations of thick spherical shell segments with variable thickness, *International Journal of Solids and Structures*, 37, 4811-4823, 2000.
- [38] K.M. Liew, L.X. Peng and T.Y. Ng, Three-dimensional vibration analysis of spherical shell panels subjected to different boundary conditions, *International Journal of Mechanical Sciences*, 44, 2103-2117, 2002.
- [39] F.B. Hildebrand, E. Reissner and G.B. Thomas, *Notes on the Foundations of the Theory of Small Displacements of Orthotropic Shells*, NACA Technical Note No. 1833, Washington, 1949.
- [40] F. Tornabene, *Meccanica delle Strutture a Guscio in Materiale Composito*, Società Editrice Esculapio, Bologna (Italy), 2012.
- [41] W. Soedel, *Vibration of Shells and Plates*, Marcel Dekker, Inc., New York, 2004.
- [42] G.B. Gustafson, *Systems of Differential Equations*, free available on <http://www.math.utah.edu/gustafso/>, accessed on 16th September 2014.
- [43] W.E. Boyce and R.C. DiPrima, *Elementary Differential Equations and Boundary Value Problems*, John Wiley & Sons, Ltd., New York, 2001.
- [44] D. Zwillinger, *Handbook of Differential Equations*, Academic Press, New York, 1997.
- [45] C. Molery and C. Van Loan, Nineteen dubious ways to compute the exponential of a matrix, twenty-five years later, *SIAM Review*, 45, 1-46, 2003.